Investigation on Positioning Techniques for Indoor Office Scenario

YUJIE ZHANG
YAN SHU
DEPARTMENT OF ELECTRICAL AND INFORMATION TECHNOLOGY
FACULTY OF ENGINEERING | LTH | LUND UNIVERSITY
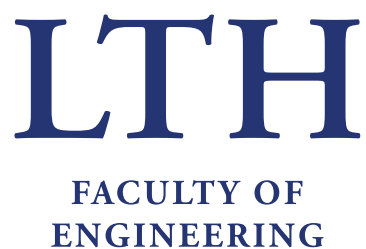
Investigation on Positioning Techniques for Indoor Office Scenario

by

Yujie Zhang
yu4266zh-s@student.lu.se

Yan Shu
ya0866sh-s@student.lu.se

Department of Electrical and Information Technology
LUND UNIVERSITY

Supervisors: Fredrik Tufvesson (EIT)
Johan Hill (Sony)
Basuki Priyanto (Sony)
Examiner: Fredrik Rusek (EIT)

30th June 2020

Abstract

This master thesis aims to investigate downlink positioning techniques and improve fifth-generation (5G) cellular positioning performance in the indoor office scenario. In the thesis work, we target in the indoor office scenario because it is a typical deployment scenario standardized in 3GPP release 16.

To analyze the positioning techniques, we develop a simulator in MATLAB. In the simulator, the channel model, environment geometry, positioning reference signals, and frame structure are all aligned with 3GPP release 16. To ensure the alignment is proper, we compare our simulation results with the results of other companies under the same conditions.

Our research mainly focuses on downlink time difference of arrival and downlink angle of departure methods. For the time difference of arrival method, we implement various techniques, such as time-based beam selection. For the angle of departure method, we apply a first delay path based angle of departure detection. The simulation results show that our receiver can obtain a more accurate measurement than the legacy methods.

Furthermore, we investigate various least squares and maximum likelihood localization algorithms. To mitigate the non line-of-sight effects, we propose an algorithm which combines the residual weighting algorithm and residual testing method. The simulation results show that this algorithm outperforms the residual weighting algorithm in the indoor office environment.

Besides, based on the maximum likelihood approach, we combine the downlink time difference of arrival technique and downlink angle of departure technique, which improves the positioning accuracy. Specifically, the positioning performance can achieve 2.9 meters and 1.1 meters of error for 80% of user equipment in the indoor mixed office and indoor open office, respectively.

Acknowledgements

List of Acronyms

3GPP   3rd Generation Partnership Project

5G   Fifth-Generation

ADS   Angular Delay Spectrum

AML   Approximate Maximum Likelihood

AoA   Angle of Arrival

AoD   Angle of Departure

AWGN   Additive White Gaussian Noise

BS   Base Station

CDF   Cumulative Distribution Function

CDL   Clustered Delay Line

CIR   Channel Impulse Response

CP   Cyclic Prefix

CRLB   Cramer-Rao Lower Bound

DFT   Discrete Fourier Transform

DL   Downlink

DL-AoD   Downlink Angle of Departure

DL-TDOA   Downlink Time Difference of Arrival

E-CID   Enhanced Cell ID

eMBB   Enhanced Mobile Broadband

ESPRIT   Estimation of Signal Parameters via Rotational Invariance Techniques

FFT   Fast Fourier Transform

FR1   Frequency Range 1

FR2   Frequency Range 2

FTs   Fixed Terminals

gNB   gNodeB

GNSS	Global Navigation Satellite System
IIoT	Industrial Internet of Things
IMT-2020	International Mobile Telecommunications-2020
IoT	Internet of Things
ITU	International Telecommunications Union
ITU-R	International Telecommunications Union Radio communication Standardization Sector
LCS	Location Services
LOS	Line-of-Sight
LS	Least Squares
LTE	Long-Term Evolution
MIMO	Multiple Input Multiple Output
ML	Maximum Likelihood
MLE	Maximum Likelihood Estimation
mMTC	Massive Machine Type Communications
mmWave	Millimetre Wave
MT	Mobile Terminal
Multi-RTT	Multi-Cell Round Trip Time
MUSIC	Multiple Signal Classification
NLOS	Non Line-of-Sight
NLS	Non-Linear Least Squares
NR	New Radio
OFDM	Orthogonal Frequency-Division Multiplexing
OTDOA	Observed Time Difference of Arrival
PAR	Peak-to-Average Ratio
PDF	Probability Density Function
PDP	Power Delay Profile
PRS	Positioning Reference signal
QPSK	Quadrature Phase Shift Keying

RAT	Radio Access Technology
RE	Resource Element
RMS	Root Mean Square
RSRP	Reference Signal Received Power
RSTD	Received Signal Time Difference
RT	Residual Testing
RTOA	Relative Time of Arrival
RWGH	Residual Weighting Algorithm
SNR	Signal to Noise Ratio
SRS	Sounding Reference Signal
TDOA	Time Difference of Arrival
TH	Threshold
TOA	Time of Arrival
TRP	Transmission and Reception Point
UE	User Equipment
UL	Uplink
UL-AoA	Uplink-Angle of Arrival
UL-TDOA	Uplink-Time Difference of Arrival
UL-RTOA	Uplink-Relative Time of Arrival
URLLC	Ultra-Reliable Low Latency Communications
WLAN	Wireless Local Area Network
WLS	Weighted Least Squares

Contents

1 Introduction

1.1 Challenges in Indoor positioning

Nowadays, different positioning techniques such as network-assisted Global Navigation Satellite System (GNSS) methods, cellular-based positioning solutions, Bluetooth positioning solutions and Wireless Local Area Network (WLAN) positioning solutions can provide real-time location to a User Equipment (UE). For outdoor environments, the embedded GNSS receiver of UEs is capable of locating the UE with good performance. However, the weak satellite signals will result in the unreliable positioning service for indoor scenarios. Hence, to provide the service with the same quality in indoor environments, telecommunication companies require other positioning alternatives. This thesis focuses on cellular positioning solutions with Downlink Time Difference of Arrival (DL-TDOA) and Downlink Angle of Departure (DL-AoD) positioning methods.

In the indoor scenario, there is typically Non Line-of-Sight (NLOS) signal propagation, which can yield the inaccurate detection of the first arrival path. Threshold-based first path detection techniques can help to measure the Time of Arrival (TOA). However, the selection of the threshold is challenging, and it directly affects the accuracy of the TOA estimate. Another challenge for TOA based positioning is the timing synchronization of different Base Stations (BSs). Practically, base stations are synchronized with GPS in many cases. The synchronization error is still in the range of [-100 ns, +100 ns] [1]. When it comes to the DL-AoD method challenge, the positioning accuracy relies on Angle of Departure (AoD) estimation, which typically depends on the beamwidth.

1.2 Methods and Objectives

Positioning techniques in 3rd Generation Partnership Project (3GPP) release 16 are required to support both regulatory and commercial requirements. Some of the commercial requirements are stringent in terms of horizontal accuracy, which poses a significant challenge for researchers in both academia and industry. The first objective of the thesis is to identify suitable DL-TDOA based positioning techniques, which includes the reference signal design, UE receiver design and localization algorithms, in order to meet the commercial requirements in the indoor office scenario. The second objective of the thesis is to analyze and provide solutions for AoD-based positioning techniques and NLOS effect mitigation. MATLAB is used as an implementation environment for the studies carried out in this thesis work. To analyze the performances of localization algorithms, we evaluate our simulation results by comparing with algorithms commonly used in 3GPP release 16.

1.3 Outline

The report is organized as follows: In Chapter 2, an overview of 5G NR is presented, which includes the introduction of three main use cases, the key features and the frame structure of 5G. Chapter 3 introduces the requirements of 5G positioning and presents several 5G positioning methods, especially the DL-AoD and OTDOA methods. Chapter 4 describes the simulation setup, and the basic experimental configuration and the procedure of the simulation. Chapter 5 validates the robustness of the thesis developed simulator by comparing with the selected results from 3GPP release 16. Chapter 6 describes the receiver design, and adaptive threshold-based TOA detection as well as the time-based beam selection method and AoD detection method. Chapter 7 describes the investigated Maximum Likelihood (ML) and Least Squares (LS) approaches. Also, this chapter investigates NLOS mitigation solutions. Chapter 8 presents and discusses the results of thesis work which includes the investigation on statistical channel properties, simulation results of the TOA and AoD estimators at UE and the evaluation results in the localization algorithms at the location server. Chapter 9 summarizes the thesis work and gives suggestions for future work.

2 5G NR Overview

This chapter gives an overview of 5G NR. The first section presents three main 5G use cases. Section 2.2 introduces the key features of 5G. Section 2.3 describes the frame structure of 5G, and the 5G numerology.

2.1 5G NR Use-cases

According to the specific requirements of 5G from the International Telecommunications Union (ITU), 5G is required to satisfy three use cases, namely Enhanced Mobile Broadband (eMBB), Massive Machine Type Communications (mMTC) and Ultra-Reliable Low Latency Communications (URLLC) [2]. These three use cases are included in International Mobile Telecommunications-2020 (IMT-2020), which is agreed by the International Telecommunications Union Radio communication Standardization Sector (ITU-R). The description of these three use cases can be seen in Table 2.1.

Table 2.1: 5G Use-cases [2].

Cases	eMBB	URLLC	mMTC
Aims	1. Enabling larger data volumes. 2. Improving user experience. Example: • Enhancing data rate.	1. Achieving very low latency. 2. Supporting high reliability. Examples: • Factory automation. • Traffic safety.	Servicing for massive number of devices. Examples: • Remote sensors. Requirements: • Low device cost. • Low device energy consumption.

2.2 5G NR features

In the previous section, the main 5G use cases are listed. To satisfy these three use cases, 5G has several new features as follows:

- 5G expands the range of the frequency spectra. The licensed-spectrum for 5G can support Frequency Range 1 (FR1) 0.45 - 6 GHz and Frequency Range 2 (FR2) 24.25 - 52.6 GHz. The higher frequency bands can support wider transmission bandwidths and associated high data rates [2].

- 5G applies a flexible OFDM numerology with different subcarrier spacing (15 kHz to 240 kHz) to support a broad range of frequency spectrum deployment [2].

- 5G utilizes up to 3300 subcarriers, and the maximum bandwidth is 400 MHz [2].

- 5G supports a low end to end latency, which is an essential feature in 5G [2].

- 5G supports multi-antenna transmission. At higher frequencies, a large number of antenna elements are used for beamforming to increase coverage. Massive MIMO is enabled at lower frequency bands to increase spectrum efficiency [2].

2.3   5G NR Numerology and Frame Structure

The numerology of 5G involves the configuration of waveform parameters, for instance, sub-carrier spacing and cyclic prefix. In [3], NR sub-carrier spacing Δf is defined as $15 \cdot 2^{\mu}$, where μ can be selected from 0 to 4. The different cyclic prefix options can be seen in Table 2.2.

Table 2.2: Supported transmission numerologies [3].

μ	$\Delta f = 15 \cdot 2^{\mu} \ [kHz]$	Cyclic prefix
0	15	Normal
1	30	Normal
2	60	Normal,Extended
3	120	Normal
4	240	Normal

Based on the 5G numerology, one 5G radio frame is defined in the unit of 10 ms [3]. One radio frame comprises of ten sub-frames where each sub-frame has 1 ms duration. The ten sub-frames are named 0 to 9. Besides, one radio frame can be divided into two equal-size half-frames [3]. Uplink and downlink have their own set of frames.

A slot consists of 14 OFDM symbols. The number of slots in a sub-frame depends on the sub-carrier spacing and cyclic prefix type. The relationship between them is summarized in Table 2.3 and Table 2.4. Note that μ is the same as in Table 2.2.

Table 2.3: Number of OFDM symbols per slot, slots per frame, slots per subframe for normal cyclic prefix [3].

μ	Number of OFDM symbols per slots	Number of slots per frame	Number of slots per subframe
0	14	10	1
1	14	20	2
2	14	40	4
3	14	80	8
4	14	160	16

Table 2.4: Number of OFDM symbols per slot, slots per frame, slots per subframe for extended cyclic prefix [3].

μ	Number of OFDM symbols per slots	Number of slots per frame	Number of slots per subframe
2	12	40	4

3 5G NR positioning

In the previous chapter, the key features of 5G were introduced. This chapter aims to introduce the 5G NR positioning methods, which are developed based on those key features. Section 3.1 explains the NR positioning requirements. The second section briefly explains a number of NR positioning methods. Since this thesis focuses on downlink positioning, the two downlink based positioning methods Downlink Time Difference of Arrival (DL-TDOA) and Downlink Angle of Departure (DL-AoD) will be presented in detail in Section 3.3 and Section 3.4, respectively.

3.1 Requirements of NR Positioning

3GPP TR 38.855 [4] specifies the regulatory and commercial requirements for NR positioning.

Regulatory requirements are identified as the minimum performance expected [4]. The specific requirements are listed below [4]:

- Horizontal positioning error should be lower than 50 meters for 80% of UEs.

- Vertical positioning error should be lower than 5 meters for 80% of UEs.

- End to end latency should be less than 30 seconds.

For commercial use cases, there are some additional requirements for indoor and outdoor deployment scenarios, which are listed as follows [4]:

- Horizontal positioning error should be lower than 3 meters of 80% UEs in indoor deployment scenarios.

- Vertical positioning error should be lower than 3 meters of 80% UEs in indoor deployment scenarios.

- Horizontal positioning error should be lower than 10 meters of 80% UEs in outdoor deployment scenarios.

- Vertical positioning error should be lower than 3 meters of 80% UEs in outdoor deployment scenarios.

- End to end latency should be less than 1 second.

Note that for commercial use cases, indoor and outdoor deployment means that UEs and gNodeBs (gNBs) are both deployed in the indoor and outdoor environment, respectively [4].

The use case family 'higher accuracy positioning' for NR is defined in [5], where it requires low latency and high reliability of the positioning information. [5] specifies that the positioning accuracy should be less than one meter in more than 95% of service areas, including indoor and outdoor environments.

3.2 Overview of Positioning Methods in 5G NR

3GPP TR 38.855 [4] introduces several types of Radio Access Technology (RAT) based positioning solutions such as DL-TDOA, Uplink-Time Difference of Arrival (UL-TDOA), Multi-Cell Round Trip Time (Multi-RTT), DL-AoD, Uplink-Angle of Arrival (UL-AoA) and Enhanced Cell ID (E-CID). Fig. 3.1 shows the structure of RAT based NR positioning. NR E-CID is a technique to enhance the UE positioning accuracy by using UE and NR radio resource related measurements [6]. In this thesis, NR E-CID will not be further discussed.
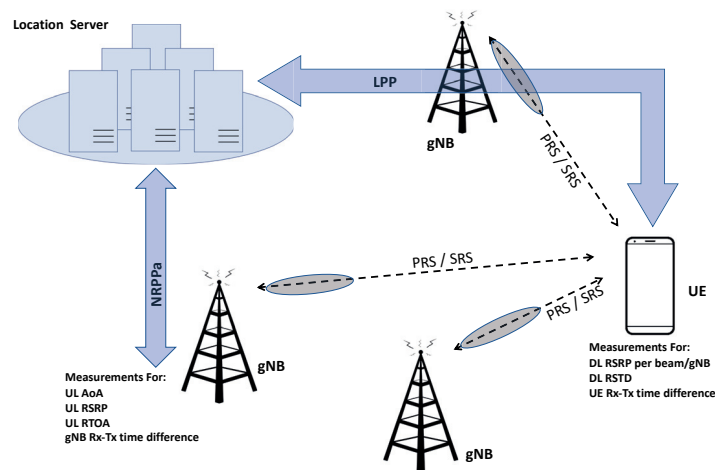
Figure 3.1: NR RAT-based positioning schemes.

Brief descriptions of DL-TDOA, UL-TDOA, Multi-RTT, DL-AoD and UL-AoA are given below.

- DL-TDOA positioning: DL-TDOA is a common NR deployed downlink positioning solution known as Observed Time Difference of Arrival (OTDOA) [6]. In NR, the Positioning Reference signal (PRS) is utilized as a reference signal to support for OTDOA positioning. The UE receives the PRS from different gNBs to measure the Received Signal Time Difference (RSTD) and report it to the location server in the core network. Then, the location server estimates the UE location by applying the RSTD and known positions of gNBs.

7

- DL-AoD positioning: DL-AoD is a positioning method which has been standardized in [6]. The structure of DL-AoD positioning is described in Fig. 3.6. Based on Reference Signal Received Power (RSRP) reported by the UE, the AoD from surrounding gNBs can be estimated, and then the estimated UE location can be triangulated by using these AoD measurements. UE can utilize received PRS signals to estimate the RSRP measurements.
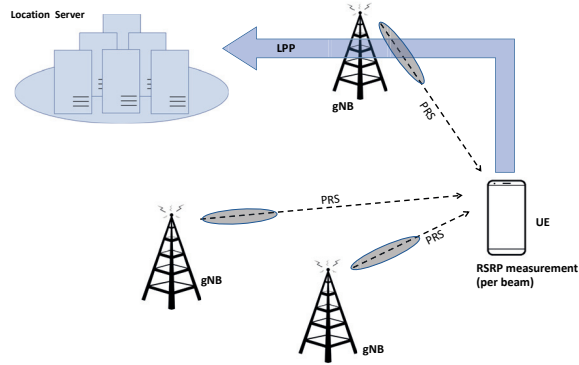
Figure 3.2: Structure of NR DL-AoD positioning.

- UL-TDOA positioning: UL-TDOA positioning method is standardized in NR [6]. According to the UL-TDOA specification, a Sounding Reference Signal (SRS) is sent by the UE to multiple gNBs. Then, gNBs measure the Uplink-Relative Time of Arrival (UL-RTOA) and send it to the location server. After that, Relative Time of Arrival (RTOA) will be used along with the known locations of gNBs to estimate the UE position.

- UL-AoA positioning: In [6], UL-AoA is specified as applying multiple Angle of Arrival (AoA) measurements to constitute the complete positioning solution. The UL-AoA positioning scheme is shown in Fig. 3.3. The Uplink (UL) SRS is used to measure azimuth of AoA and zenith of AoA at gNBs [6]. There exists some available algorithms that can support AoA estimation, for instance, Multiple Signal Classification (MUSIC), Estimation of Signal Parameters via Rotational Invariance Techniques (ESPRIT), and Discrete Fourier Transform (DFT) algorithms [7]. Once the location server receives the AoA measurements, a triangulation method can be applied in the location server to estimate the UE position.

- Multi-RTT positioning: Multi-RTT is round trip time measurement through the Downlink (DL) PRS, and UL SRS transmitted from gNBs and UEs [6]. The Multi-RTT positioning scheme can be seen in Fig. 3.4. After the round trip time reported to the location server, the estimated distance between gNBs and UEs can be computed. After that, the method for UE position estimate is similar with the other methods using a trilateration algorithm. Although the Multi-RTT method can reduce the effect from synchronization error, the high cost of Multi-RTT is still an issue for the practical deployments [8].
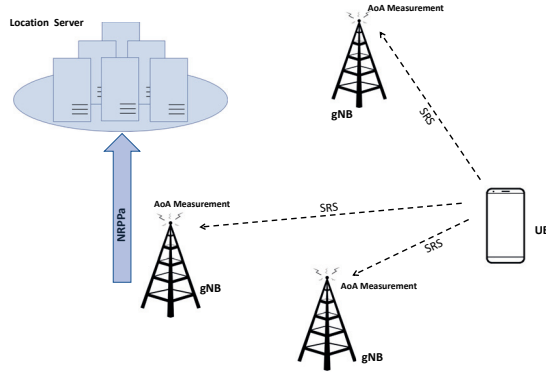
Figure 3.3: Structure of NR UL-AoA positioning.
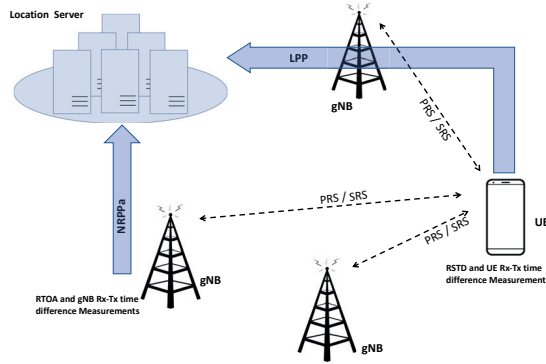
Figure 3.4: Structure of NR Multi-RTT positioning.

3.3 OTDOA positioning

OTDOA is a positioning method that applies a multiateration technique [6]. The OTDOA positioning method is illustrated in Fig. 3.5, where three gNBs nearby the UE are activated. The local time of three gNBs is synchronized through GPS before the start of PRS transmission. After that, three gNBs transmit the PRS simultaneously to the UE. Based on the received signals, UE measures three TOAs: $\tau 1, \tau 2, \tau 3$. The measurement from one of gNBs is considered as a reference. In Fig. 3.5, the reference is gNB$_1$, and two Time Difference of Arrival (TDOA) measurements can be formed as $t_{2,1} = \tau_2 - \tau_1, t_{3,1} = \tau_3 - \tau_1$. After that, the UE sends the measured TDOA information back to the location server from which the position and the relative error estimates are made. Each TDOA provides possible locations laying on a hyperbolic curve. By finding the intersection of these hyperbolic curves in Fig. 3.5, the location server estimates the position of the UE in the grey shaded area.
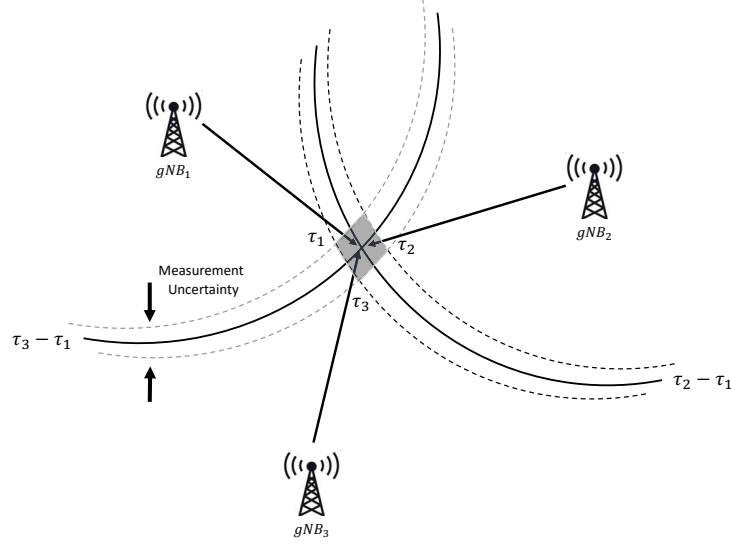
Figure 3.5: Multilateration in NR OTDOA Positioning.

3.3.1 Positioning Reference Signal Configuration

The 5G PRS is mainly used in the OTDOA positioning method [3]. PRS can be applied to estimate TDOA between different gNBs. To map the PRS into different Resource Elements (REs) in one subcarrier with 14 OFDM symbols, each PRS comprises a Quadrature Phase Shift Keying (QPSK) modulated pseudo-random sequence. Each generated sequence is determined by the slot number, cell ID, OFDM symbol and Cyclic Prefix (CP). According to [3], the PRS in NR is based on a length-31 Gold sequence, which has good correlation properties. The generated reference sequence can be described as [3]

$$r(m) = \frac{1}{\sqrt{2}}(1 - 2c(2m)) + j\frac{1}{\sqrt{2}}(1 - 2c(2m + 1)). \tag{3.1}$$

The initial state of $c(m)$ in NR can be expressed as

$$c_{\text{init}} = \left(2^{22} \left\lfloor n_{\text{ID,seq}}^{\text{PRS}}/1024 \right\rfloor + 2^{10}(N_{\text{symbl}}^{\text{slot}} n_{s,f}^{\mu} + l + 1)(2(n_{\text{ID,seq}}^{\text{PRS}} \mod 1024) + 1) + (n_{\text{ID,seq}}^{\text{PRS}} \mod 1024) \right) \mod 2^{31}. \tag{3.2}$$

Here, $n_{s,f}^{\mu}$ is the slot number, l is the OFDM symbol within the slot and the downlink PRS ID $n_{\text{ID,seq}}^{\text{PRS}}$ which is included in 0, 1, …, 4095 [3]. After the generation of reference sequence, it is allocated to the resource element as

$$\alpha_{k,l}^{(p,\mu)} = \beta_{\text{PRS}} r(m), \tag{3.3}$$

$$k = mK_{\text{comb}}^{\text{PRS}} + \left((k_{\text{offset}}^{\text{PRS}} + k') \mod K_{\text{comb}}^{\text{PRS}} \right), \tag{3.4}$$

$$l = l_{\text{start}}^{\text{PRS}}, l_{\text{start}}^{\text{PRS}} + 1, \cdots, l_{\text{start}}^{\text{PRS}} + L_{\text{PRS}} - 1, \tag{3.5}$$

where β_{PRS} is a scale factor for $r(m)$, l is the symbol number in time domain and k represents the subcarrier number in frequency domain [3]. Further, $l_{\text{start}}^{\text{PRS}}$ denotes

the first symbol of DL PRS within a slot, L_{PRS} in $2, 4, 6, 12$ indicates the number of symbols that can be allocated for DL PRS resources, $K_{\text{comb}}^{\text{PRS}}$ is the comb size which can be selected among $2, 4, 6, 12$, $k_{\text{offset}}^{\text{PRS}}$ is the resource-element offset that is defined from 0 to $K_{\text{comb}}^{\text{PRS}}$ and the frequency offset k' is the function of $l - l_{\text{start}}^{\text{PRS}}$ as show in following Table 3.1.

Table 3.1: The frequency offset k' as a function of $l - l_{\text{start}}^{\text{PRS}}$ [3].

$k_{\text{comb}}^{\text{PRS}}$	Symbol number in DL PRS resource $l - l_{\text{start}}^{\text{PRS}}$											
	0	1	2	3	4	5	6	7	8	9	10	11
2	0	1	0	1	0	1	0	1	0	1	0	1
4	0	2	1	3	0	2	1	3	0	2	1	3
6	0	3	1	4	2	5	0	3	1	4	2	5
12	0	4	3	9	1	7	4	10	2	8	5	11

3.3.2 Reference Signal Time Difference

RSTD is specified in [6], which can support OTDOA positioning method. The definition of RSTD is the relative time difference between reference gNodeB (gNB) j and measured gNB i, calculated as

$$RSTD = T_{\text{subframe},j} - T_{\text{subframe},i}, \tag{3.6}$$

where $T_{\text{subframe},j}$ represents to the time when the UE receives a start of the subframe from gNB j and $T_{\text{subframe},i}$ corresponds to the time when the UE receives a start of the subframe from gNB i.

3.3.3 Time of Arrival

As mentioned before, OTDOA is calculated based on several measured TOAs. The distance between the gNB and the UE can be easily computed from the TOA with the knowledge of the speed of light.

The TOA estimation quality is dependent on the extent of time synchronization of the system, as well as the influence of multipath propagation. Any tiny time synchronization error will affect the positioning accuracy. For accurate TOA estimation, clock synchronization between gNBs and UEs is required. In real systems, GPS is used for gNBs to achieve clock synchronization through satellites. Additionally, the environment may cause NLOS propagation, such as multipath and scattering effects. The specific TOA estimation will be discussed in Chapter 6.

3.3.4 Time Difference of Arrival

TDOA is an improved positioning method based on TOA estimation, and is the basis of OTDOA positioning. It only requires time synchronization between gNBs instead of between gNBs and UEs. TDOA positioning approaches can determine

the UE position by calculating the time difference between the different received signals from multiple gNBs. In practice, each TDOA determines one hyperbola. Ideally, several different hyperbolae intersect at one point, which is the desired position.

3.4 DL-AoD positioning

Fig. 3.6 defines the zenith angle θ and azimuth angle ϕ. The zenith angle represents the angle between z-axis and the direction of arrival. The azimuth angle is formed between x-axis and projection of direction on xy-plane.
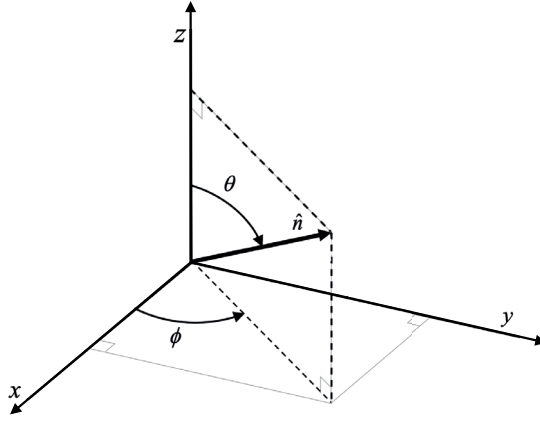
Figure 3.6: Definition of azimuth angle ϕ and zenith angle θ.

When applying DL-AoD, at least two gNBs need to be used to estimate the location of the UE. Assuming the known locations of gNBs are denoted as $X_i = (x_i, y_i, z_i)$, where $i = 0, 1, ..., K-1$ and K is the number of used gNBs. Besides, the UE location can be expressed as $X_{UE} = (x_{UE}, y_{UE}, z_{UE})$. The main idea of DL-AoD method is to estimate the angle from gNBs to the UE in the downlink. Following this coordinate system, measured azimuth angle and zenith angle are modelled as

$$\hat{\phi}_i = \phi_i + \varepsilon_i \tag{3.7}$$

$$\hat{\theta}_i = \phi_i + \eta_i \tag{3.8}$$

where ε_i and η_i denote the estimated angle errors. Regarding these two error elements, it is assumed they are independent and identically distributed (i.i.d) Gaussian parameters with zero mean and σ_i^2, $\sigma_i'^2$ variance. Note that in order to estimate the position of UE, it is necessary to know the absolute direction of the antenna array at the gNBs [9].

After obtaining the measured $\hat{\phi}_i$ and $\hat{\theta}_i$, the Maximum Likelihood Estimation (MLE) for the UE position $\hat{X}_{UE}$ can be expressed as

$$\hat{X}_{UE} = \underset{X_{UE}}{\mathrm{argmax}}\, p(X_{UE}|\hat{\phi}_1, ..., \hat{\phi}_{K-1}; \hat{\theta}_1, ..., \hat{\theta}_{K-1}). \tag{3.9}$$

4 Simulation Setup

This chapter describes the details of our simulation setup. Section 4.1 introduces the indoor office scenario. Section 4.2 describes the antenna model. Section 4.3 explains the Clustered Delay Line (CDL) channel models. Then, Section 4.4 and Section 4.5 define the Line-of-Sight (LOS) probability and pathloss, respectively. In the last section, the simulator is described.

4.1 Indoor Office Scenario

The selected indoor office has 120 meters length, 50 meters width and 3 meters height [10]. The layout of the indoor office can be seen in Fig. 4.1.
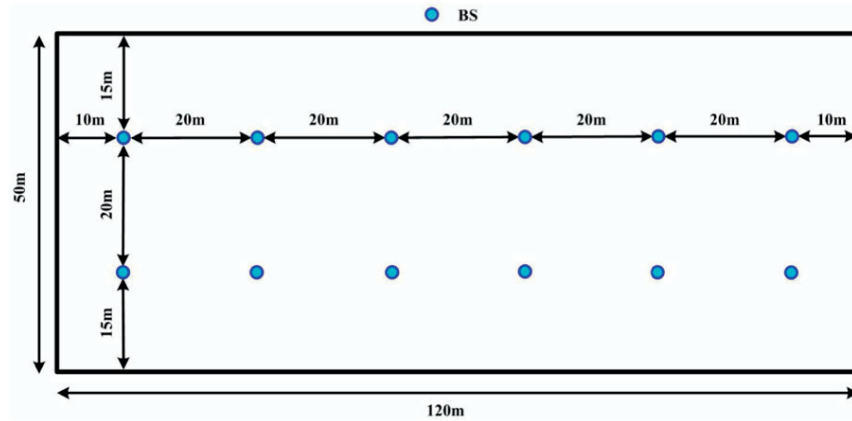
Figure 4.1: Layout of indoor office [10].

The blue dots in Fig. 4.1 are locations of gNBs. The distance between two gNBs is 20 meters. Also, the height of gNBs is 3 meters, i.e. they can be seen as mounted on the ceiling of the indoor office. Besides, in the simulation, the UE is uniformly located in this area. The height of every dropped UE is 1.5 meters, and the mobility is set to 3 km/h, where the mobility affects the Doppler frequency and fading.

4.2 Antenna Model

In the thesis work, the antenna of the UE is assumed to be omnidirectional. The gNB antenna, shown in Fig. 4.2, is modelled as a uniform rectangular panel array,

including $M_g N_g$ panels , where M_g is the number of panels in one column and N_g represent the number of panels in one row [10]. In this model, the antenna panels are uniformly distributed with a specific spacing $d_{g,H}$ and $d_{g,V}$ in the horizontal direction and vertical direction, respectively. Besides, N represents the number of columns, M is the number of antenna elements with the same polarization in each column [10]. Moreover, the antenna panel can be set as single polarized (P = 1) or dual polarized (P = 2) [10].

In the thesis work, the setting of the antenna model is as in [4]. The antenna is configured as $(M, N, P, M_g, N_g) = (4, 8, 2, 1, 1)$ and $d_{g,H} = d_{g,V} = 0.5$.
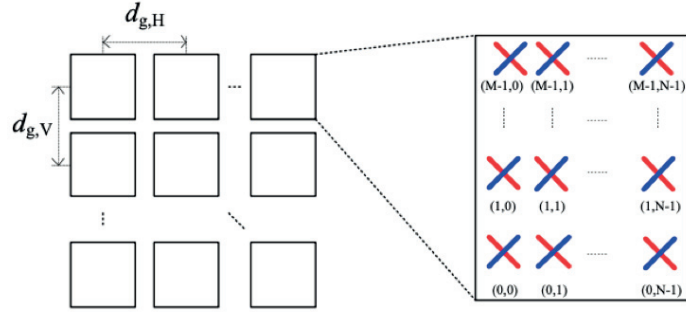
Figure 4.2: Cross-polarized panel array antenna model [10].

4.3 Channel Model

Our simulation applies the CDL channel models for NLOS and LOS situations. The CDL channel models are introduced for the whole frequency range between 0.5 GHz and 100 GHz with a maximum 2 GHz bandwidth [10]. There are five different CDL channel models: CDL-A, CDL-B, CDL-C, CDL-D and CDL-E, each profile can be found in Appendix A. Among them, CDL-A, CDL-B and CDL-C represent NLOS cases, while the other two represent LOS cases. Note that a single CDL model represents a certain channel realization.

For LOS CDL models CDL-D and CDL-E, the K-factor values can be modified according to specific requirements. The desired K-factor of a model is denoted as K_{desired} [dB]. For the Laplacian clusters of CDL-D and CDL-E, the cluster powers are set by

$$P_{n,\text{scaled}} = P_{n,\text{model}} - K_{\text{desired}} + K_{\text{model}}, \qquad (4.1)$$

where $P_{n,\text{scaled}}$ and $P_{n,\text{model}}$ represent the scaled path power and the model path power of cluster n [10]. Besides, the K_{model} is determined as [10]

$$K_{\text{model}} = P_{1,\text{model}}^{\text{LOS}} - 10 \log_{10} \left(\sum_{n=1}^{N} 10^{P_{n,\text{model}}/10} \right). \qquad (4.2)$$

4.4 Line-of-Sight Probability

As mentioned above, the five CDL channel models are representing LOS or NLOS cases. According to [10], we utilize the LOS probability to apply LOS or NLOS CDL channel models in the indoor mixed and open office. The different equations of the LOS probability of the indoor mixed and open office can be found in (4.3) and (4.4), respectively.

$$Pr_{\text{LOS}} = \begin{cases} 1, & d_{\text{2D-in}} \leq 1.2 \text{ m} \\ \exp\left(-\frac{d_{\text{2D-in}}-1.2}{4.7}\right), & 1.2 \text{ m} \leq d_{\text{2D-in}} < 6.5 \text{ m} \\ \exp\left(-\frac{d_{\text{2D-in}}-6.5}{32.6}\right), & 6.5 \text{ m} \leq d_{\text{2D-in}} \end{cases} \qquad (4.3)$$

$$Pr_{\text{LOS}} = \begin{cases} 1, & d_{\text{2D-in}} \leq 5 \text{ m} \\ \exp\left(-\frac{d_{\text{2D-in}}-5}{70.8}\right), & 5 \text{ m} \leq d_{\text{2D-in}} < 49 \text{ m} \\ \exp\left(-\frac{d_{\text{2D-in}}-49}{211.7}\right) & 49 \text{ m} \leq d_{\text{2D-in}}. \end{cases} \qquad (4.4)$$

In (4.3) and (4.4), $d_{\text{2D-in}}$ is the horizontal distance between the UE and gNBs in the indoor area, which is defined in Fig. 4.3.
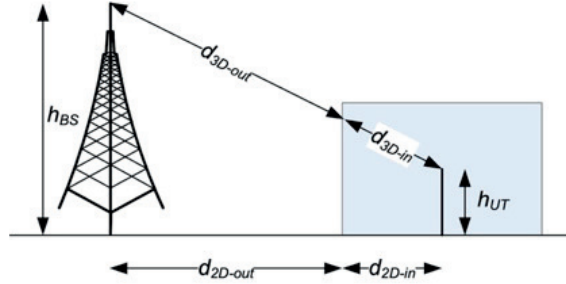
Figure 4.3: Definition of $d_{\text{2D-in}}$ for indoor area [10].

4.5 Pathloss

Pathloss is the average decline of power density when the electromagnetic wave propagates in space. It is an essential part of the link budget in the telecommunication system design. As [10] defined, for indoor office scenario, the pathloss model can be divided into LOS and NLOS cases. For LOS cases, the pathloss can be modeled as

$$\text{PL}_{\text{LOS}} = 32.4 + 17.3\log_{10}(d_{\text{3D}}) + 20\log_{10}(f_c), \ 1 \text{ m} \leq d_{\text{3D}} \leq 150 \text{ m}, \ \sigma_{\text{SF}} = 3, \quad (4.5)$$

where σ_{SF} means the standard deviation of shadow fading, d_{3D} represents the the distance between gNBs and the UE in the three-dimensional space [10]. In NLOS cases, the pathloss can be calculated as [10]

$$\text{PL}_{\text{NLOS}} = \max(\text{PL}_{\text{LOS}}, \text{PL}'_{\text{NLOS}}), \ 1 \text{ m} \leq d_{\text{3D}} \leq 150 \text{ m}, \ \sigma_{\text{SF}} = 8.03. \qquad (4.6)$$

Here, in (4.6),PL'_{NLOS} can be expressed as [10]

$$\mathrm{PL}'_{\mathrm{NLOS}} = 38.3 \log_{10}(d_{\mathrm{3D}}) + 17.30 + 24.9 \log_{10}(f_c), 1 \text{ m} \leq d_{\mathrm{3D}} \leq 150 \text{ m}, \ \sigma_{\mathrm{SF}} = 8.03. \tag{4.7}$$

Note that f_c is the center frequency which is normalized by 1 GHz, and distance values are normalized by 1 m [10].

4.6 Simulation Procedure
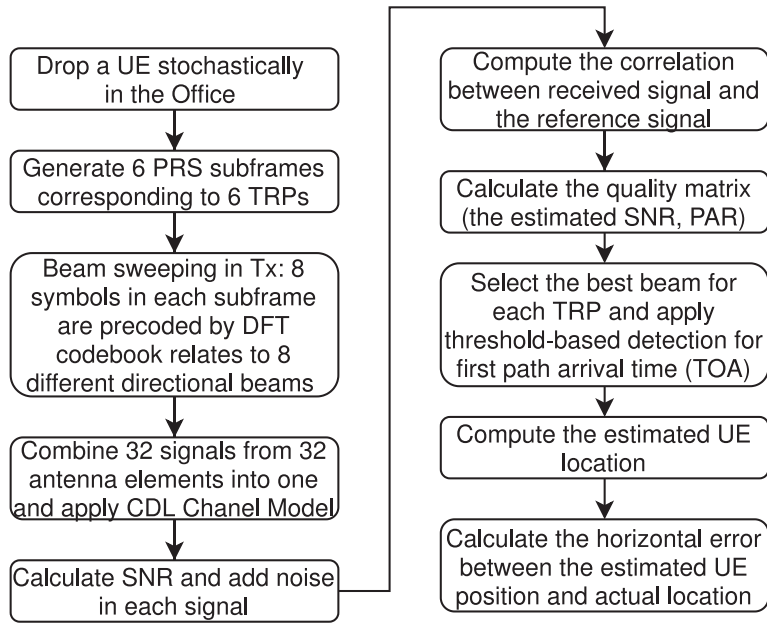
Figure 4.4: Simulation Procedure.

Fig. 4.4 shows the basic simulation procedure of our simulator. In the beginning, the UE is randomly dropped in the area. Then, the six closest Transmission and Reception Points (TRPs) generate PRS signals and transmit them to the UE. Here, we call the gNB as the Transmission and Reception Point (TRP). The reason for only using six closest TRPs is that the resource block configuration of the PRS apply a comb-6 mapping structure, which defines a frequency reuse factor of 6 and allows six different TRPs to transmit PRS signals to the UE simultaneously. The frequency-time grid is shown in Fig. 4.5, where each colour grid represents the PRS transmitted from one of six different TRPs. Fig. 4.5 shows that there are a total of eight used symbols in one subframe. There is also a procedure called beam sweeping, this method allows TRPs to transmit beams in 8 different predefined directions in order to identify the strongest one for TOA estimation. The reason for using eight symbols is that eight different beams correspond to 8 symbols in one subframe. After beam sweeping, 32 signals from 32 antenna elements are combined together. In the simulation, we apply the CDL channel model in the combined signal. The power of

17

the additional noise is calculated in Fig. 4.6. When calculating the Signal to Noise Ratio (SNR) for different UEs, it follows

$$\text{SNR} = 105 \text{ dBm} - \text{PL}(d_{\text{3D}}) + 10\log_{10}(n), \ n = 1, 4, \tag{4.8}$$

where n is determined by the 100 MHz or 400 MHz bandwidth.
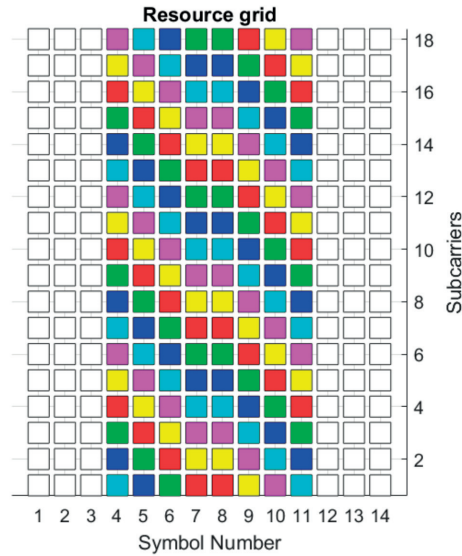
Figure 4.5: Simulation Resource Grid.

At the UE side, correlation is performed between the received signal and the reference signal. Then, the UE computes the quality matrix for the best beam selection and applies the threshold-based method for TOA detection. When the location server receives TOAs from the UE, it calculates the UE location.
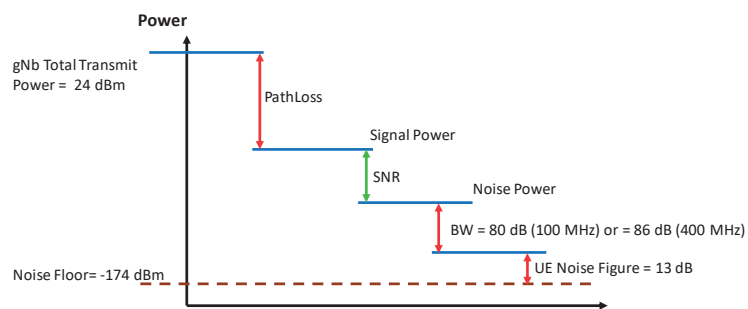
Figure 4.6: Link Budget.

5 Simulation Validation

This chapter validates our simulator. We compare the simulation results of our simulator with the results from [4]. Section 5.1 and Section 5.2 describe the two comparisons of simulation results.

5.1 Company 1

This section describes the specific configurations of Company 1 [11] and thesis developed simulator. Besides, this section shows the comparison results between Company 1 and our simulator.

5.1.1 Configuration 1

According to [4], the specific parameters of Company 1 are focused on the 30 GHz carrier frequency, 120 GHz subcarrier spacing and 100 MHz reference signal transmission bandwidth. The other parameters can be found in Table 5.3. The simulation environment is indoor office, which has 12 TRPs in the ceiling of the office. Company 1 uses a total of 36 sectors from 12 TRPs. However, our simulator initially utilizes only the six closest TRPs and selects one beam from one sector of each TRP. Hence, for the comparison of the results, we set the same parameters as Company 1.

5.1.2 Results Comparison 1

The results of Company 1 are given in Table 5.1 [4]. The second-row in Table 5.1 represents the positioning errors in the units of meters. The result of Company 1 at 80% of UEs only has a 1.99-meter error in the horizontal direction, which fulfils the positioning requirement that [4] specified.

Table 5.1: Positioning Results from Company 1 [4].

Percentile	50	60	70	80	90
FR2, 100 MHz, perfect Sync	1.02	1.24	1.54	1.99	3.21

We plot the results of our simulator and Company 1 in Fig. 5.1. In our simulation, a total of 7000 UEs are simulated. Our simulation results are very close to the results of Company 1. Also, both results are almost overlapped around 80% of UEs. The real difference between the two results may be triggered by the different number of simulated UEs.
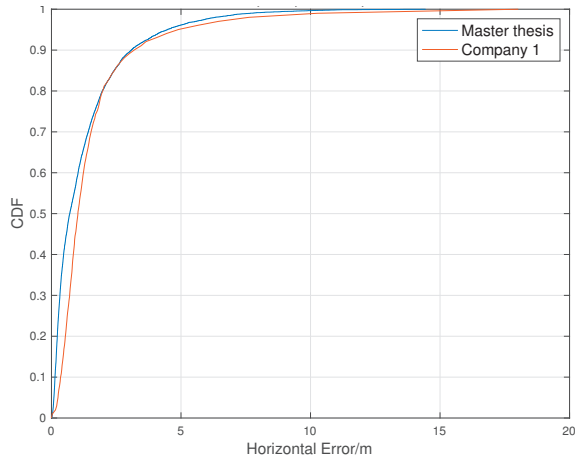
Figure 5.1: Result comparison between thesis developed simulator and Company 1 in indoor office.

5.2 Company 2

This section describes the specific configurations of Company 2 [12] and our simulator. Also, results comparisons are shown in this section.

5.2.1 Configuration 2

The specific configurations of Company 2 [4] and our simulator are shown in Table 5.4. Company 2 uses a different allocation type of resource blocks, namely the comb-1 mapping structure. To align with Company 2 configurations, we modify our simulator to apply the same configurations.

As shown in Table 5.4, there are two different transmission bandwidths are set by Company 2. Since Company 2 only mentions that they use 12 TRPs in Table 5.4, we assume that Company 2 applies 36 sectors in the simulation.

5.2.2 Results Comparison 2

Table 5.2 shows the results of Company 2. The second-row and third-row in the table represent the positioning errors in the units of meters.

The comparison between our simulator and Company 2 with 100 MHz bandwidth is shown in Fig. 5.2. As can be seen from Fig. 5.2, the results of our simulator are a little bit better than the results of Company 2. The possible reason is that Company 2 only uses one symbol per occasion, but we use eight symbols. Fig. 5.3 shows the comparison of the results in 400 MHz bandwidth, and our simulator performs similar results to Company 2 at 80% of UEs.

Table 5.2: Result from Company 2 [4].

Percentile	50	67	80	90	95
DL-TDOA, FR2, 400 MHz, Perfect Sync	0.4	0.8	1.6	4.2	9.5
DL-TDOA, FR2, 100 MHz, Perfect Sync	1.2	1.8	2.9	5.3	8.6
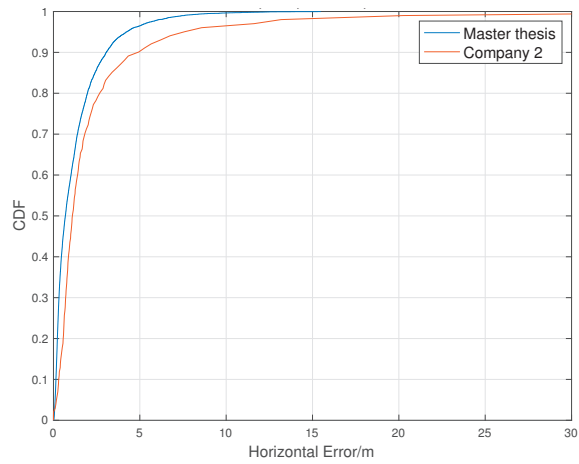
Figure 5.2: Results comparison with Company 2 in indoor office (100 MHz Bandwidth).
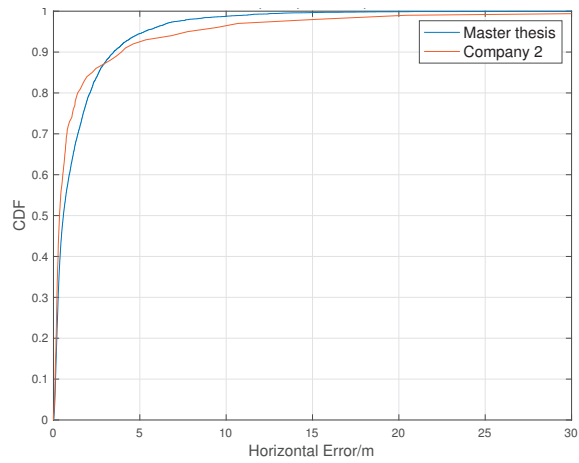
Figure 5.3: Results comparison with Company 2 in indoor office (400 MHz Bandwidth).

Table 5.3: Specific parameters comparison between master thesis and Company 1.

Parameter	Master thesis	Company 1
Channel Model	3GPP TR 38.901 [10]	3GPP TR 38.901 [10]
Carrier frequency	30 GHz	30 GHz
Subcarrier spacing	120 kHz	120 kHz
Reference signal Transmission Bandwidth	100 MHz/400 MHz	100 MHz
Reference signal physical structure and resource allocation (RE pattern) (reference to figure in contribution)	Comb-6/Comb-1	Comb-6
Reference signal (type of sequence, number of ports,...)	PRS: Gold, 1-port	PRS: Gold, 1-port
Number of sites	36 sectors/12 sites	36 sectors/12 sites
Number of symbols used per occasions	8	8
Number of occasions used per positioning estimate	1	1
Power-boosting level	0 dB	0 dB
Interference modelling (ideal muting, or other)	Ideal muting	Ideal muting
Description of measurement algorithm (e.g. super resolution cancellation,...)	Threshold-based first path detection	Threshold-based algorithm for the first arrival path (FAP) estimation
Description of positioning technique/ applied positioning algorithm (e.g. Least squares, Taylor series, etc)	Only consider the measurement with the highest PAR among 8 beams, Least square	Taylor based, measurements above -15 dB are used for positioning
Network synchronization assumption	No sync error	No sync error
Beam-related assumption (Beam sweeping/alignment assumption at the Tx and Rx sides)	Tx sweeping	Tx sweeping
Precoding assumptions	DFT codebook	Signal Tx port

Table 5.4: Specific parameters comparison between master thesis and Company 2.

Parameter	Master thesis	Company 2
Channel Model	3GPP TR 38.901 [10]	3GPP TR 38.901 [10]
Carrier frequency	30 GHz	30 GHz
Subcarrier spacing	120 kHz	120 kHz
Reference signal Transmission Bandwidth	100 MHz/400 MHz	100 MHz/400 MHz
Reference signal physical structure and resource allocation (RE pattern) (reference to figure in contribution)	Comb-6/Comb-1	Comb-1
Reference signal (type of sequence, number of ports,...)	PRS: Gold, 1-port	PRS: Gold, 1-port
Number of sites	36 sectors/12 sites	36 sectors/12 sites
Number of symbols used per occasions	8	1
Number of occasions used per positioning estimate	1	1
Power-boosting level	0 dB	0 dB
Interference modelling (ideal muting, or other)	Ideal muting	Ideal muting
Description of measurement algorithm (e.g. super resolution cancellation,...)	Threshold-based first path detection	TOA estimation without oversampling with TOA pruning before the positioning engine using the ratio of the estimated TOA peak over the median of the channel energy response (CER)
Description of positioning technique/ applied positioning algorithm (e.g. Least squares, Taylor series, etc)	Only consider the measurement with the highest PAR among 8 beams, Least square	For DL-TDOA pick the best between Taylor series, and Chan's algorithm.
Network synchronization assumption	No sync error	No sync error
Beam-related assumption (Beam sweeping/alignment assumption at the Tx and Rx sides)	Tx sweeping	The best beam pair is identified based on the criteria of receiving the earliest path given that the received power is larger than a threshold.
Precoding assumptions	DFT codebook	Kronecker product between vertical and horizontal weight vectors takenfrom DFT, with oversampling factor r.

6 UE Receiver Design

This chapter mainly introduces a UE receiver structure for the 5G NR positioning. Section 6.1 derives a signal model. After that, in Section 6.2, the correlator design is introduced. Section 6.3 illustrates a threshold-based peak detection method for the TOA estimation. The last section explains the AoD detection method.

As introduced in Chapter 4, 12 gNBs were available in our indoor office setup. However, in the thesis work, only 6 gNBs are used in order to avoid interference. The thesis work follows an assumption that a location server can detect the nearest 6 gNBs around the UE in advance.

The role of the UE is to detect the TOAs from the PRS signals transmitted by the nearby gNBs. Generally, the detection has two steps. Firstly, the receiver estimates the channel impulse response from the correlation between the received PRS signal and the reference signal. Secondly, the UE applies an algorithm to find the delay of the first path.

Below is a flow chart of the TOA estimation and AoD estimation:
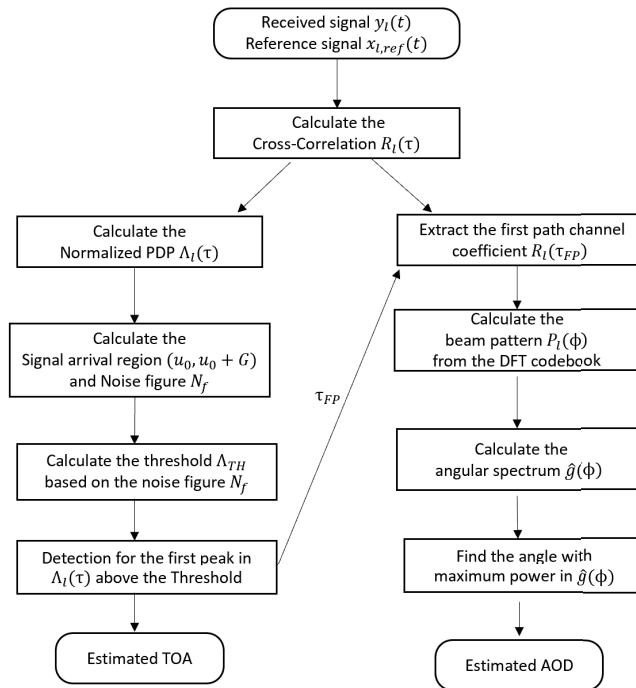
Figure 6.1: Flow chart of the TOA estimation and AoD estimation.

6.1 Received Signal model

In time domain, the n-th sample in the l-th OFDM symbol is denoted as

$$x_l(n), n \in [-G, N - 1], \; l \in [0, N_{\text{symb}} - 1], \qquad (6.1)$$

where G is the length of CP, N is the size of Fast Fourier Transform (FFT), and N_{symb} is the number of OFDM symbols within one time slot. The CP is the duplicate of the last G samples of the OFDM symbol, $x_l(n) = x_l(n + N), \; n \in [-G, N - 1]$.

As described in our simulation setup from Chapter 4, the TRPs are equipped with 4 by 8 MIMO antennas and the UE use omnidirectional antenna. For simplifying our model and reducing the computational complexity, we assume that the UE antenna elements from a TRP would be blocked by the same obstacles. As a result, the Channel Impulse Response (CIR)s from all the TRP antenna elements are the shifted versions of each other. The phase shifts are determined by the element spacing and AoA.

In the indoor office environment, most of the objects are steady. Therefore, it assumes that the channel is time-invariant. Time invariance means the CIR does not change fast over the time domain. Under this assumption, within a time slot, the CIRs applied to each symbol are the same.

The CIR in each time instant can be denoted as $h(0), ..., h(N-1)$. Then, the received signal $y_l(n)$ can be expressed as

$$y_l(n) = \sum_{i=0}^{L-1} h(n)x_l(n - i - \tau) + z_l(n), \; n \in [-G, N + L + \tau - 1], \qquad (6.2)$$

where τ is the propagation delay of the signal, which is the parameter related to the TOA, and $z_l(n) \sim CN(0, \sigma^2)$ is the additive complex Gaussian noise.

6.2 CIR estimation

The correlator plays an important role at the receiver side, since it is used to estimate the CIR. In the thesis work, a time domain correlator is used, which estimates the CIR by calculating the cross-correlation function between the received signal and the transmitted signal in the time domain.

In the design of the time-frequency resource grid, eight symbols out of 14 are occupied with PRS. We design a correlator for processing the resource grid symbol by symbol. Before the transmission of the PRS signal, a pilot signal carrying the Cell-ID of TRPs, the index of the closest sector, and the DFT codebook are sent in

advance to inform UE. By knowing this information, UE rebuilds the transmitted signal and prepares for the cross-correlation at the next step.

The mathematical expression of an unbiased form of cross-correlation is given by

$$R_l[n_\tau] = \frac{1}{M - |n_\tau|} \sum_{i=n_\tau}^{L_\tau} x_{l,\text{ref}}(i) y_l^*(i - n_\tau), \tag{6.3}$$

where the $R_l[n_\tau]$ is the cross-correlation, the index n_τ can translate to the delay by dividing the sampling frequency. l is the index of the symbol and M refers to the FFT size. $x_{l,\text{ref}}$ is the reference signal, which can be derived from the (6.17). Here, $*$ is the complex conjugation operator.

In FR2 numerology, the FFT size is set to 4096. A direct way to calculate the computation complexity is by counting the number of complex multiplication. It is assumed that the maximum delay of interest is L_τ. The number of the complex multiplication is approximate to $4096^2 L_\tau$, from which one can observe that the complexity linearly increases with the range of the delay of interest. In other words, the complexity can be reduced by setting the L_τ properly.

The thesis work proposes a L_τ based on the geometry of the indoor office by (6.4). The scope is limited by the maximum dimension of the room to cover all the possible LOS components in the delay domain.

$$L_\tau = \lceil 2D_{\max} f_s / c \rceil \approx 440, \tag{6.4}$$

where f_s is the sampling frequency, c is the speed of light, and $D_{\max}$ denotes the maximum dimension of the office which is given by

$$D_{\max} = \sqrt{\text{width}^2 + \text{length}^2}. \tag{6.5}$$

The cross-correlation is normalized to approximate the PDP which can be regarded as the normalized absolute value of the estimated CIR. The x_l is assumed to have an ideal auto-correlation property. The power of the transmit signal is denoted as P_x to simplify the analysis. Then the correlation can be modeled as a function of the real CIR by (6.6). Here, the channel is assumed to be time-invariant as well. Therefore, all the h_l remain the same in the delay domain.

Additionally, since beamforming is applied and the symbols in a time slot have different array gains, the h_l in the spatial domain would differ.

$$R_l(\tau) = P_x \, h_l(\tau, \theta) + R_{\text{res},l}(\tau), \tag{6.6}$$

where $R_{\text{res},l}(\tau)$ represents the residual noise and interference resulting from correlation between x_l and y_l. The $h(\tau, \theta)$ is the CIR with respect to delay and the angle of departure.

To facilitate the comparison among different CIRs, scaling all the cross-correlation into the same manner is needed. The Power Delay Profile (PDP) is given by

$$\begin{aligned}
\Lambda_l(t) &= |R_l(t)|^2 / \max(|R_l(t)|^2) \\
&= C(|h_l(t - \tau, \theta)|^2 + \sigma^2),
\end{aligned} \tag{6.7}$$

where the $\Lambda_l(t)$ is the PDP of the channel, the $\max(*)$ is the operation extracting the maximum value, C is a constant value, and σ is the standard deviation of the cross-correlation noise.

6.3   Peak detection

The goal of the TOA estimation is to detect the LOS path delay through the PDP of the channel. The PDP can be simplified into a delay tapped model. The method to figure out which tap is the LOS path is still a challenging topic in the research field.

In this section, a method for TOA detection from the PDP is given in [13]. The detection follows by three steps. Firstly, the UE receiver detects the signal arrival region for estimating the noise floor as well as the SNR level. After that, an adaptive threshold-based first tap detection is applied to estimate the delay of the LOS path. Finally, the UE receiver refines the delay measurement.

6.3.1   Signal arrival region determination

For a multipath channel, the signal arrival region contains multiple taps corresponding to the taps of the channel. A moving sum for the window size of CP length is then computed as (6.8) [14], where the G denotes the length of the CP.

$$\Lambda_{\mathrm{win}}(k) = \sum_{t=k}^{k+G-1} \Lambda(t), \ u \in [0, G-1] \tag{6.8}$$

The signal is regarded as arrived in the time region:

$$u_0 \le t \le u_0 + G - 1, \ \text{where } u_0 = \operatorname{argmax}_u \{\Lambda_{\mathrm{win}}(u)\}. \tag{6.9}$$

At the region $t < u_0$ or $t > u_0 + G - 1$, only the noise term occurs. The noise power, also called the noise floor, can be calculated by averaging the terms outside of the signal region. The estimated noise floor N_f is considered as the σ^2 term in (6.6). As confirmed by much research, the moving window method can reliably detect the signal region [13]. The UE receiver uses the estimated noise floor to calculate the SNR in the next step.

6.3.2 Adaptive threshold-based first peak detection

Mathematically, the attained PDP is a shifted version of the autocorrelation of the transmitted signal when the channel has a single delay tap. The delay of the signal is the position of the only tap. However, in a multipath channel, more than one tap would occur. From a physical point of view, the direct transmission path is shorter than other reflected paths. Therefore, the LOS path is likely to be the position of the first peak. However, the searching for the first peak sometimes does not lead to a correct measurement because noise and interference may also cause some peaks.

Distinguishing the peak from the signal and the peak from the noise becomes problematic in the receiver design. A threshold is applied to filter out the unwanted noise to address this issue. Given the threshold, the criterion for the delay can be expressed by (6.10). The linear constraint $u_0 \leq t < u_0 + G - 1$ is to make sure that the delay is in a range of the signal arrival region. To fulfill the unlinear constraints $\Lambda_l(t) \geq \Lambda_{\text{th}}$ and $\Lambda_l(t-1) \leq \Lambda_l(t) \leq \Lambda_l(t+1)$, the power in one time instant has to be higher than the threshold value and higher than the nearby values.

$$\tau = \min_{\substack{u_0 \leq t < u_0 + G - 1 \\ \Lambda_l(t) \geq \Lambda_{\text{th}} \\ \Lambda_l(t-1) \leq \Lambda_l(t) \leq \Lambda_l(t+1)}} t, \tag{6.10}$$

where the Λ_{th} is the threshold.

A way to set up the threshold is by making it adaptive to the signal power and noise power [13]. The model of it can be defined as

$$\Lambda_{\text{th}} = \alpha \left(\beta \, \Lambda_{l,\max} + (1 - \beta) \, N_f \right), \tag{6.11}$$

where the α is a design parameter, the β is a constant trading off between the noise floor and the metric peak. α and β are determined through simulations, to have a trade-off for different channels and different SNRs.

Fig. 6.2 is an example of the adaptive threshold based first peak detection.

In the NLOS channel, the first path in the delay domain is no longer the one with the maximum power. In some of the cases, the first path position is a bit ahead of the tap with maximum power. How to set up the threshold properly becomes a problem. If the threshold is too high, the LOS path would be filtered out by the threshold. On the contrary, if the threshold is too low, some unfiltered noise term ahead of the LOS path may be captured and lead to a wrong detection. During the thesis, these two behaviours are given by names, called overdetermination and underdetermination. Overdetermination occurs when the threshold filters out the wanted tap. Underdetermination occurs when the threshold can not filter out the noise tap. In Chapter 8, the rate of overdetermination and underdetermination as a function of the threshold (β) will be discussed.
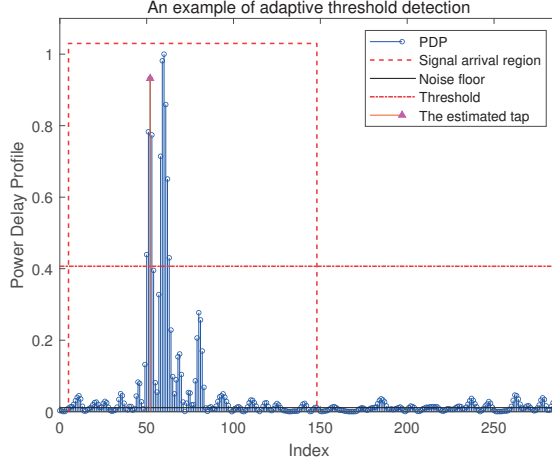
Figure 6.2: An example of adaptive threshold-based first peak detection, $\beta = 0.4$, $\alpha = 1$.

6.3.3 Refinement for TOA measurement

After peak detection, The UE receiver selects one specific tap. The position of the detected tap may not be the actual delay in some of the cases. In the thesis work, the sampling rate used is 500 MHz. Due to the limit of the sampling rate, the actual tap of the first arriving path may lie on the left or the right side of the detected tap. The error by the resolution limit is around $\pm 1/2 f_{\text{samp}} = \pm 1 \ ns$. A step can reduce this error. A simple and effective method is by smoothing average for the detected tap and its neighbouring taps, for example, over ten taps:

$$\tau' = \frac{\sum_{t=\tau-5}^{\tau+5} t\Lambda(t)}{\sum_{t=\tau-5}^{\tau+5} \Lambda(t)}. \tag{6.12}$$

6.4 gNB Tx Beam Sweeping

Defined by [4], FR2 specifies the gNB antenna set up in an indoor office scenario. Each gNB is equipped with with a 3-sector antenna. Each sector is a N by M MIMO antenna. N and M are the number of elements in a column and row, respectively. When considering the array gain of the MIMO system, beam-forming is used to focus the signal in a particular direction rather than having the signal spread in all directions from the transmitter antenna.

Since the UE location is unknown, it is of interest to use beam-sweeping to search for all directions in the horizontal plane and select one beam pair with the best signal quality. In the thesis work, the transmitter only uses the horizontal beams. Each row of elements in the array is considered a uniform linear array and transmits the same horizontal beam. A way to realize it is to apply the DFT codebook to each

of the symbols in a time slot [15] [16]. The number of beams is set to 8 corresponding to 8 different symbols. Each of the beams can cover 15°.

The DFT-based beamforming weight vector codebook for the antenna array with M elements is given by

$$\mathbf{w} = [1 \quad \exp(-j\pi cos\theta_m) \quad ... \quad \exp(-j\pi(M-1)cos\theta_m)]^T, \tag{6.13}$$

where the m is the index of the antenna element and θ_m is the angle of interest.

In the thesis work, the beam is spread over $30°$ to $150°$ in the Location Services (LCS); therefore, θ_m for each symbol is denoted as

$$\theta_{m,\text{LCS}} = 30° + m(150° - 30°)/15 \in [37.5°, \ 52.5° \ ...142.5°]. \tag{6.14}$$

The response of the beamformer, which is also known as the beam pattern, can be given by

$$P(\theta) = \sum_{m=0}^{M-1} w_m^* \exp(-j2\pi f_c \tau_m) = \mathbf{w}^H \mathbf{d}, \tag{6.15}$$

where the τ_m is the propagation delay for the signal from sensor 0 to sensor M and is a function of τ. The f_c is the center frequency [17]. $(\cdot)^H$ is the hermitian transpose. Correspondingly, the $\mathbf{d}$, which is known as steering vector can be denoted as

$$\mathbf{d} = [1 \quad \exp(-jw\tau_1) \quad ... \quad \exp(-j2\pi f_c \tau_{M-1})]^T. \tag{6.16}$$

The beam patterns of the eight different beams are given in Fig. 6.3. Each of the beams has approximately 12 dB gain in the main lobe, and the sidelobes are suppressed.

The spatial distribution of the antenna gain, a polar plot of 8 different beams is shown in Fig. 6.4. The eight symbols in a time slot would be sent through these 8 beams accordingly. The output $x(t)$ of the beamformer at time t is given by an instantaneous linear combination of these spatial samples $s_l(t), l \in [0, N_{\text{symb}} - 1]$, as

$$x_l(t) = \sum_{m=1}^{M-1} s_l(t)w_m^* = \mathbf{w}^H s_l, \tag{6.17}$$

where the $s_l(t)$ and $x_l(t)$ are the input and output of the beamformer, l is the index of the symbol.
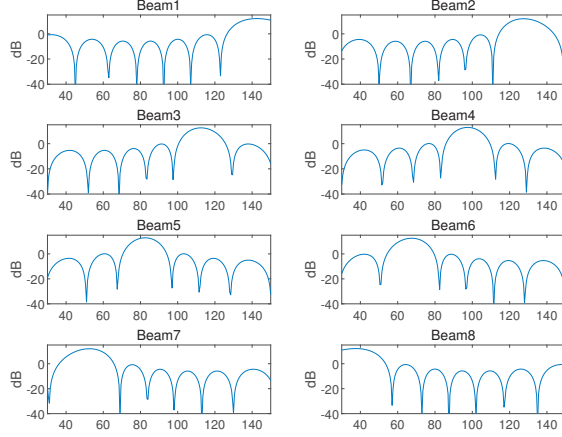
Figure 6.3: Beam pattern of 8 different beams, the y axis is in unit dB.

6.5 Beam quality measurement

Since beam sweeping is applied in each TRPs, UE would receive symbols carried by the different beams. According to the study from the previous section, the beam pointing to the UE direction would have an approximate 12 dB antenna gain. This beam tends to have a better TOA measurement than the others.

For selecting the best beam, a quality matrix is built to qualify the beams received by the UE. Then, the beam with the best quality would be picked and considered as the best beam. The TOA and AoD estimated from it are regarded as the most reliable measurement. An evaluation for the performances from these eight different methods is given in Chapter 8. The detailed description is given by Table 6.1.

The methods 'TOA1' and 'TOA2' is by selecting the beam with the shortest TOA estimate. A similar TOA-based beam selection method can be found in [11]. Since the TOA estimate is sometimes smaller than the first path delay, a proposed constraint for the TOA estimate is applied. In 'TOA1' method, the TOA estimate without the range $\overline{\text{TOA}} \pm \sigma_{\text{TOA}}$ would be filtered out. In 'TOA2' method, a wider range is applied for comparison, which is $\overline{\text{TOA}} \pm \sigma_{\text{TOA}}$. In [18], the selection is based on the RSRP. [12] suggests using SNR, MPMR, and FPMR methods. Additionally, it is of interest to investigate the difference between PDP medium and the average PDP average. Methods MPAR and FPAR are proposed to compare with the methods MPMR and FPMR.
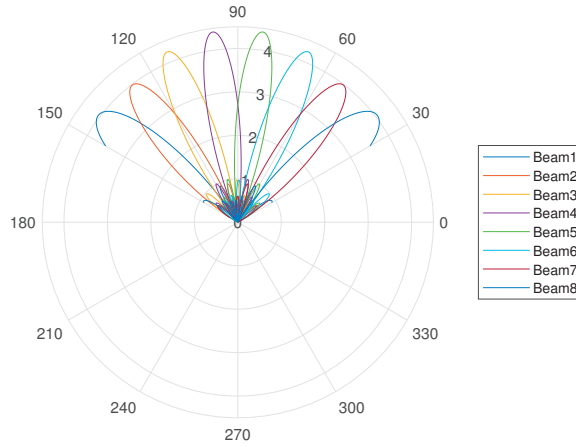
Figure 6.4: Polar plot of 8 different beam. The r axis is the antenna gain of signal amplitude. Each beam would cover $15°$.

6.6 AoD detection

One of the benefits of using the MIMO antennas in the TRP side is to allow the location server to obtain the spatial information for high accuracy estimation of the UE location. A conventional and direct way of the AoD measurement is by searching for the angle of the beam with the maximum power. More specifically, at a specific time, UE measures the average output power over a symbol in a particular direction. Among different directions, it selects the one with maximum power.

However, the accuracy of the estimated AoD crucially relies on the beamwidth of the beam patterns, and the estimation error becomes larger when the beamwidth increases. For the TRP antenna in FR2 specification, eight horizontal antenna elements in one sector give a $15°$ resolution, which can cause a significant AoD error.

The angular delay channel can be modelled by

$$h_l(\tau, \phi) = g(\tau, \phi) \, P_l(\phi) + v_l, \tag{6.18}$$

where $P_l(\phi)$ is the beam pattern of the l-th spatial filter given by (6.15), $g(\tau)$ is the complex coefficients depending on channel fading and receive antenna gain, v_l is the channel estimation error and is assumed to be i.i.d. Gaussian distributed noise following $N(0, \sigma_h^2)$.

In a multi-cluster channel, the channel impulse response $h_l(\tau, \phi)$ is a superposition of different path. Only the LOS paths contain the AoD information. Therefore, the objective of AoD detection is to extract the AoD information only from the first path, which is the most likely the LOS path.

In the thesis work, the first path delay obtained from the TOA estimator can be used in AoD detection. The complex value at the first path delay τ_{FP} in the cross-

Table 6.1: 8 different ways to qualify beams.

Beam selection methods	Description
TOA1	the beam with the shortest TOA estimate which satisfies $|\text{TOA} - \overline{\text{TOA}}| < 2\sigma_{\text{TOA}}$
TOA2	the beam with the shortest TOA estimate which satisfies $|\text{TOA} - \overline{\text{TOA}}| < 10\sigma_{\text{TOA}}$
SNR [12]	the beam with the largest estimated SNRs given by $\overline{\Lambda_l(\tau)} \, / \, N_f$
MPAR	the beam with the largest main peak to average ratio: $1 \, / \, \overline{\Lambda_l(\tau)}$
MPMR [12]	the beam with the largest main peak to median ratio: $1 \, / \, \text{median}(\Lambda_l(\tau))$
FPAR	the beam with the largest first peak to average ratio: $\Lambda_l(\tau_{\text{FP}}) \, / \, \overline{\Lambda_l(\tau)}$
FPMR [12]	the beam with the largest first peak to median ratio: $\Lambda_l(\tau_{\text{FP}}) \, / \, \text{median}(\Lambda_l(\tau))$
RSRP [18]	the average of the signal power over a symbol

correlation $R_l(\tau_{FP})$ (from (6.3)) can be denoted as

$$\hat{h}_l(\tau_{FP}, \phi_{UE}) = R_l(\tau_{FP}) = \hat{g}(\tau_{FP}, \phi_{UE}) \, P_l(\phi_{UE}) + v_l, \qquad (6.19)$$

where ϕ_{UE} is the AoD pointing to UE.

Note that UE can obtain M measurements $\left\{ \hat{h}_l(\tau_{FP}, \phi_{UE}), \, l = 1, 2, ..., M \right\}$. For convenience, the $\hat{h}_l(\tau_{FP}, \phi_{UE})$ is denoted as $\hat{h}_l$.

To estimate $g(\phi)$, a least-squares method is applied by (6.20). In DL positioning, beam sweeping is applied in the gNBs, and the UE would measure the AoD. It assumes that the UE knows the beam patterns $P_l(\phi)$ in advance. The equation can be regarded as taking a weighted average operation over eight beam patterns. The weight in here is the average power of the beam [19].

$$\hat{g}(\phi) = \frac{\sum_{l=1}^{N_{\text{symb}}} P_l(\phi) \hat{h}_l}{\sum_{l=1}^{N_{\text{symb}}} \left| \hat{h}_l \right|^2} \qquad (6.20)$$

where the $\hat{h}_l$ is a complex value calculated by the integration of the PDP over the time domain.

With the estimated angular spectrum $g(\phi)$, the AoD can be estimated as the angle with maximum amplitude. Fig. 6.5 gives an example of the AoD detection 6.5. In the indoor office positioning, the AoD measurement is mainly for the azimuth angle. For further research, this method can be extended to the zenith angle where

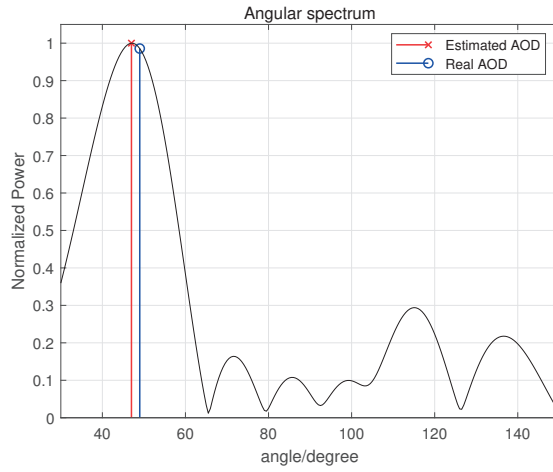the beam pattern and the estimated channel are on zenith direction accordingly.

Figure 6.5: An example of an estimated angular spectrum, the estimated AoD is given by the angle with the maximum amplitude.

7 Localization Algorithms

Localization algorithms are used to estimate the UE location from the measured TDOA or AoD. Algorithms using the TDOA measurements from different base stations have been studied extensively in the literature [20]. Various localization algorithms with different performances, computational complexities, the prior knowledge requirements, and different levels of robustness against NLOS bias effects have also been reported.

The main objective of 3GPP [4] is to improve the localization accuracy. The accuracy is evaluated as the horizontal error for 80% of the UEs. The challenge of the thesis is to provide a robust solution not only for LOS cases but also to include the NLOS cases. The office geometries can be summarized into two types: open office and mixed office. The UE-gNB links in both scenarios have a probability of being blocked. The detailed description of the channel can be found in Chapter 4. In the thesis, we assume that the location server has prior knowledge of the office. The prior knowledge includes the the standard deviation of the TOA error and the AoD error. In practice, the information can be obtained from channel measurements in advance.

This chapter introduces ten different localization algorithms. Table 7.1 present a the summary of them. The algorithms can be classified into two types. The first one is ML, which is by searching for the best estimate having the largest probability. The second one is LS, which is by searching for the best estimate having the smallest residual error. A TOA-based ML method is derived in [21]. The thesis work modified this method and extend it to a TDOA-based method, a AoD-based method and a hybrid TDOA+AoD ML method. In [22], A non-linear LS method called Residual Weighting Algorithm (RWGH) is derived in this chapter to mitigate the NLOS effect.

All the mentioned methods are to solve the optimization problems of the non-linear form cost function. Some research derives a linear approach to reduce complexity. In [21], a linear ML method called AML algorithm is given. In [23], a TDOA linear LS method is derived, which is also called Chan's algorithm. In [24], an AoD-based linear LS method and a hybrid TDOA+AoD linear LS method are proposed.

This chapter firstly gives a comprehensive introduction of different commonly used TDOA-based localization algorithms. After then, a proposed method for NLOS mitigation is introduced. At the end of the chapter, the AoD-based and the hybrid TDOA+AoD solution are given.

Table 7.1: Localization Algorithms.

	Non-Linear	Linear
Maximum Likelihood (ML) Approach	• TDOA ML • AoD ML • Hybrid TDOA+AoD ML	• AML algorithm [21]
Least Squares (LS) Approach	• TDOA Nonlinear LS • AoD Nonlinear LS • Residual weighting [22] algorithm	• Chan's algorithm [23] (TDOA Linear LS) • AoD Linear LS [24] • Hybrid TDOA+AoD Linear LS [24]

7.1 System model for TDOA-based location solution

Consider a wireless system with N TRPs, $\hat{\mathbf{x}} = [\hat{x}, \hat{y}]^T$ is the estimation of the UE location and $\mathbf{x}_i = [x_i, y_i]^T$ is the position of the i-th TRP. For each of the TRPs, the UE can obtain one TOA measurement and one AoD measurement, which is denoted as τ_i and ϕ_i. The estimated distance between TRPs and UEs $\hat{r}_i$ is modeled in (7.1) and (7.2). From the measurement in Chapter 8, the SNR of the receiver signal from LOS or NLOS links can be approximated as a Gaussian distribution. The accuracy of TOA measurements is greatly affected by the SNR. Hence, in the estimated TOA model, the LOS noise term n_i and the NLOS noise term b_i can also be assumed to be Additive White Gaussian Noise (AWGN).

$$\hat{d}_i = d_i + b_i + n_i = c\tau_i, \tag{7.1}$$

where c is the speed of light, d_i is the real distance between the i-th TRPs and UE, $n \sim N(0, \sigma_i^2)$ is the AWGN with variance σ_i^2, and b_i is a introduced positive distance bias due to the blockage of direct path given by

$$b_i = \begin{cases} 0 \text{ , if the } i\text{-th TRP is LOS}, \\ \psi_i \text{ , if the } i\text{-th TRP is NLOS}, \end{cases} \tag{7.2}$$

where the bias term $\psi_i \geq 0$ can be modelled in different ways depending on the channel.

Let

$$\mathbf{d} = [d_1, d_2, ..., d_N]^T \tag{7.3}$$

be a vector of actual distances between the Mobile Terminal (MT) and the Fixed Terminals (FTs),

$$\hat{\mathbf{d}} = [\hat{d}_1, \hat{d}_2, ..., \hat{d}_N] \tag{7.4}$$

be a vector of estimated distances, and

$$\mathbf{b} = [b_1, b_2, ..., b_N]^T \tag{7.5}$$

be a bias vector. Also let

$$\mathbf{Q} = \mathrm{E}[\mathbf{nn}^T] = \mathrm{diag}[\sigma_1^2, \sigma_2^2, ..., \sigma_N^2] \tag{7.6}$$

to denote the covariance of noise vector $\mathbf{n} = [n_1, n_2, ..., n_N]^T$ with the assumption that all the noise terms are zero mean and independent Gaussian random variables, where diag is the operator that returns a square diagonal matrix with the elements of input vector on the main diagonal.

The distance between i-th TRP and UE, d_i, can be calculated by the real coordinate of the TRP and UE, as

$$(x - x_i)^2 - (y - y_i)^2 = d_i^2 \ , \ i = 1, 2, ..., N. \tag{7.7}$$

Similarly, if any errors or noises exist, the estimated distance can not be calculated the exact coordinate of the UE. The estimated form is given by

$$(\hat{x} - x_i)^2 - (\hat{y} - y_i)^2 = \hat{d_i}^2 \ , \ i = 1, 2, ..., N. \tag{7.8}$$

For the TDOA measurements, let

$$\mathbf{d} = [d_{21}, d_{31}, ..., d_{ij}, ...]^T \tag{7.9}$$

be the vector form of the difference between d_i and d_j which

$$d_{ij} = d_i - d_j \ , \ i, j = 1, ..., N \ , \ i \neq j. \tag{7.10}$$

Additionally, in order to have a more compact form of expressions, it is defined that

$$k = x^2 + y^2 \ , \ k_i = x_i^2 + y_i^2. \tag{7.11}$$

7.2 TDOA-based solution

7.2.1 TDOA Maximum Likelihood algorithm

ML algorithm searches for the best estimate that maximizes the conditional probability of the hypothesis UE location given by the TDOA measurement $\hat{d}$. TDOA ML algorithms are divided into two different types: with or without reference TRP. The TDOA is calculated by two of the TOA estimates. Without reference TRP means the algorithm considers all the possible TDOAs. To reduced the complexity, one of the TOA is regarded as the reference, and ML would use the TDOAs calculated from the other TOAs and the reference TOA.

TDOA ML without reference TRP

If the number of the TOA estimate is N, there would be C_2^N possible combinations of TOA pairs and also C_2^N possible TDOA measurements. Here, C is the combination operator given by $C_k^n = \frac{n!}{(n-k)!\,k!}$.

Derived in (7.12), in the absence of NLOS bias, the conditional Probability Density Function (PDF) for a given TDOA measurements $\hat{d}$ is a function of the hypothesis of UE location x. Here, it assumes that the noise of the TOA estimate is Gaussian distributed. Accordingly, the difference between two TOAs (i.e. TDOA) is also regarded as Gaussian distributed. The variance of a TDOA is the sum of the variances of the two TOA estimates.

$$P(\hat{\mathbf{d}}|\mathbf{x}) = \prod_{\substack{i,j=1,\dots,N \\ i>j}} \frac{1}{\sqrt{2\pi(\sigma_i^2 + \sigma_1^2)}} \exp\left[-\frac{(\hat{d}_{ij} - \tilde{d}_{ij})^2}{2(\sigma_i^2 + \sigma_j^2)} \right], \qquad (7.12)$$

where σ is the standard deviation of the TOA estimate times the speed of light, $\hat{d}_{ij}$ is the difference between TOA measurements from the i-th TRP and the one from the j-th TRP times the speed of light. $\tilde{d}_{ij}$ is the hypothesis TDOA given by the hypothesis UE location x, which can be given by

$$\tilde{d}_{ij} = \sqrt{(x - x_i)^2 + (y - y_i)^2} - \sqrt{(x - x_j)^2 + (y - y_j)^2}. \qquad (7.13)$$

Then, the solution of the ML approach is the one that maximizes the probability density $P(\hat{\mathbf{d}}|\mathbf{x})$, as

$$\hat{\mathbf{x}} = \arg\max_{\mathbf{x} \in \mathbf{C}} P(\hat{\mathbf{d}}|\mathbf{x}), \qquad (7.14)$$

where $\mathbf{C}$ is the constrain of the estimated UE location.

To solve (7.14), searching over all the possible UE locations is required which make the ML approach computationally intensive.

TDOA ML with reference TRP

If one of the TRP is considered as the reference TRP, denoted as TRP1, the total number of the possible TDOAs is $N - 1$. The conditional probability is given by (7.15). In addition, the equation can be extended to a matrix form.

$$P(\hat{\mathbf{d}}|\mathbf{x}) = \prod_{i=2}^{N} \frac{1}{\sqrt{2\pi(\sigma_i^2 + \sigma_1^2)}} \exp\left[-\frac{(\hat{d}_{i1} - \tilde{d}_{i1})^2}{2(\sigma_i^2 + \sigma_1^2)}\right]$$
$$= \frac{1}{\sqrt{(2\pi)^N \det(\mathbf{Q}_d)}} \exp\left(\frac{J}{2}\right), \tag{7.15}$$

where the matrix $\mathbf{Q}_d$ is a $(N-1)$ by $(N-1)$ noise matrix which is given by

$$\mathbf{Q}_d = \mathrm{diag}[(\sigma_1^2 + \sigma_2^2), \, (\sigma_1^2 + \sigma_3^2), ..., (\sigma_1^2 + \sigma_N^2)]^T, \tag{7.16}$$

and J is given by

$$J = [\hat{\mathbf{d}} - \mathbf{d}]^T \mathbf{Q}_d^{-1} [\hat{\mathbf{d}} - \mathbf{d}]. \tag{7.17}$$

The thesis work mainly studies the TDOA ML without reference TRP. To avoid confusion, the term 'TDOA ML' means the TDOA ML without reference TRP.

(7.15) provides a way to transfer the residual error $(\hat{d}_{i1} - \tilde{d}_{i1})^2$ into the probability which can be applied to visualize the distribution of the likelihood given by each TDOA measurement. Noting that in (7.15), there are $N-1$ terms in the product. Each of them can be regarded as the PDF given by only TRP1 and TRPi. Examples of the distribution maps and their summation are presented in Fig. 7.1.
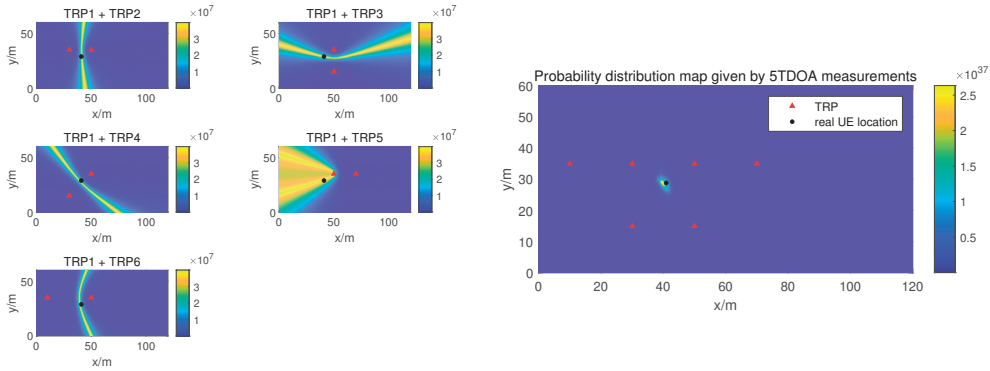
Figure 7.1: TDOA ML gives PDF with reference TRP. The left figure is an example of a probability density distribution map given by the TDOA the N-th TRP and the reference TRP. The joint probability of the 5 PDF distribution maps for AoD measurement is the right figure. The standard deviation of the TOA measurement is set to 3.3 m.

From Fig. 7.1, one can observe that the locations fit for one specific TDOA measurement yield to a hyperbolic line between two TRPs. The sum of the five subplots is the right figure from which one can obtain the final decision of the UE location. The location, the yellow dot in Fig. 7.1, is most likely be the UE location.

7.2.2 Approximate Maximum Likelihood Algorithm

Since the ML method is computationally intense, an approximate method Approximate Maximum Likelihood (AML) algorithm can reduce the complexity, which is proposed in [21]. At the beginning of the AML algorithm, the first estimate of the UE location is calculated by

$$\mathbf{x} = \frac{1}{2}(\mathbf{D}^T \, \mathbf{Q}_d^{-1} \, \mathbf{D})^{-1} \, \mathbf{D}^T \, \mathbf{Q}_d^{-1}(v_1 + d_1 \mathbf{\Psi}), \tag{7.18}$$

where

$$\mathbf{D} = \begin{pmatrix} x_1 - x_2 & y_1 - y_2 \\ \vdots & \vdots \\ x_1 - x_N & y_1 - y_N \end{pmatrix}, \mathbf{\Psi} = 2[\hat{d}_{21} \ \cdots \ \hat{d}_{N1}]^T, \tag{7.19}$$

and

$$\mathbf{\Psi} = 2[\hat{d}_{21} \ \cdots \ \hat{d}_{N1}]^T. \tag{7.20}$$

Note that the d_1 is the variable related to the location of the UE. In the beginning, an initial guess of the UE location is used as the input d_1. The solution of it is the first estimated UE location x. Then, AML takes the first estimation from the first step to calculate the weighted matrix $\mathbf{\Phi}$, which is

$$\mathbf{\Phi} = \mathbf{W}\mathbf{\Lambda}, \tag{7.21}$$

where

$$\mathbf{W} = \left[\frac{\partial \mathbf{d}(\mathbf{x})}{\partial \mathbf{x}}\right]^T \mathbf{Q}_d^{-1} \mathbf{W} = \left[\frac{\partial \mathbf{d}(\mathbf{x})}{\partial \mathbf{x}}\right]^T \mathbf{Q}_d^{-1}, \tag{7.22}$$

and

$$\mathbf{\Lambda} = \text{diag}\left[\frac{1}{(d_2 + d_1 + \hat{d}_{21})} \ \cdots \ \frac{1}{(d_N + d_1 + \hat{d}_{N1})}\right]. \tag{7.23}$$

The second step of AML is to utilize the weight to calculate a more refined location by

$$\mathbf{x} = \frac{1}{2}(\mathbf{\Phi}\mathbf{D})^{-1}\mathbf{\Phi}(v_1 + d_1 \mathbf{\Psi}). \tag{7.24}$$

Following (7.18) gives a updated value of **x**. Repeating (7.24) with time value **x** by 5 more times to obtain the final estimation UE location.

The simulation shows that AML performs much faster and more capable than the ML solution, but the tradeoff is of lower accuracy. Especially in the NLOS cases, the AML would have several meters error more than ML.

7.2.3   TDOA Non-Linear Least Square

The method of LS is a standard approach in regression analysis to approximate the solution of overdetermined systems (sets of equations in which there are more equations than unknowns) by minimizing the sum of the squares of the residuals.

Least squares techniques in positioning, similar to the maximum likelihood, start with the evaluation of the residual error of all the possible UE location from different TRPs. The difference between the two detectors is that in ML detector, it transfers the error into probability and obtains the one hypothesis UE location with the highest likelihood. However, the LS detector finds the one with the minimum residual error.

The Non-Linear Least Squares (NLS) is a robust technique for estimating an unknown parameter when its probability distribution is unknown. It is also one of the conventional methods for positioning given by [25]. The best estimate in the NLS minimizes the sum of squared residuals (a residual being: the difference between an observed value, and the hypothesis value provided by a model). The detection criterion is

$$
\begin{aligned}
\hat{\mathbf{x}} &= \arg\min_{\mathbf{x}\in\mathbf{C}} R_{\mathrm{es}}(\mathbf{x}) \\
&= \arg\min_{\mathbf{x}\in\mathbf{C}} \left\{ \sum_{\substack{i,j=1,\dots,N \\ i>j}} \beta_i (\hat{d}_{ij} - \tilde{d}_{ij})^2 \right\},
\end{aligned}
\tag{7.25}
$$

where $R_{\mathrm{es}}(\mathbf{x})$ is the residual error corresponding to the UE location. β_i is the weight to characterize the reliability of each link, which yields to the Weighted Least Squares (WLS). If no prior information about the channel is available, β_i set to 1. To avoid confusion, the thesis work names the LS detector with equal weight, NLS.

In some of the researches, the closest TRP, also called TRP1, is regarded as the reference in the residual calculation. One of the reasons is that those methods dedicated to the positioning among cells, which is a legacy method from LTE communication. In a cell scenario, the distance from UE to BS inside the cell is smaller than the distance from UE to the neighbour cell. Therefore, the measurement from the TRP closest to UE is usually is much powerful than others. In the indoor scenario, the situation is different. First of all, the SNR difference among the closest TRPs would not have so much differences. Besides, the differences among the TDOA pairs are small.

When considering the NLOS cases, the selection of the reference TRP would tremendously affect the accuracy. If TRP1 is an NLOS TRP, the measured TOA from it would be off from the correct value. If this TRP1 is regarded as the reference, all TDOAs derives from the TOA1 have a significant error. For reliability, instead of using reference, all the combinations with two TRPs are used to calculate the TDOA. The i and j in the detection criterion (7.25) are the indexes of the TRPs in combinations. There will be C_2^N terms in the polynomial of residual.

The thesis work solves the non-linear form of the cost function by iteration refinement in which the system would keep adjusting the probable UE location depending on the residual error. In the simulator, when the difference between the current iteration and the previous one is smaller than 0.01 times the initial residual, the iteration stops.

Since the NLS method has a decent performance in the simulation, in the thesis work, the NLS method is considered a reference compared with other algorithms.

7.2.4 Linear Least Squares Algorithm

Due to the high complexity of the NLS methods, a linear form of least square algorithm is preferable for some of the systems requiring high response speed and low computation capacity. [23] proposes a linear approach of LS methods, which is known as 'Chan's algorithm.' To cancel the non-linear terms, Chan assumed that the distance from UE to the TRP1 r_1 is independent of x and y. Then the residual error vector can be derived as

$$\psi = \mathbf{h} - \mathbf{G}_a \mathbf{z}_a^o, \tag{7.26}$$

where $\mathbf{z}_a^o = [x, y, r_1]^T$ is the unknown vector which in the first iteration is the initial guess of the UE's location. The constant matrix $\mathbf{h}$ and $\mathbf{G}$ are

$$\mathbf{h} = \begin{bmatrix} d_{2,1}^2 - K_2 + K_1 \\ d_{3,1}^2 - K_3 + K_1 \\ \vdots \\ d_{N,1}^2 - K_N + K_1 \end{bmatrix}, \ \mathbf{G}_a = - \begin{bmatrix} x_{2,1} & y_{2,1} & d_{2,1} \\ x_{3,1} & y_{3,1} & d_{3,1} \\ \vdots & \vdots & \vdots \\ x_{N,1} & y_{N,1} & d_{N,1} \end{bmatrix}. \tag{7.27}$$

From the above equation, the UE location can be solved, from (7.26). As a refinement, the inverse of covariance matrix $\mathbf{Q}_d^{-1}$ can be used to weight the distribution given by each link:

$$\hat{\mathbf{x}} = (\mathbf{G}_a^T \mathbf{Q}_d^{-1} \mathbf{G}_a)^{-1} \mathbf{G}_a^T \mathbf{Q}_d^{-1} \mathbf{h}. \tag{7.28}$$

7.3 Cramer-Rao lower bound for TDOA ML

CRLB expresses a lower bound on the variance of unbiased estimators of a determ-inistic parameter. Given the conditional PDF of $\hat{d}$ as in (7.12) , we derive the CRLB for the TDOA ML estimator. In the thesis work, CRLB can help to predict the theor-etical lower bound of the variance of the estimated UE location error given by the TDOA MLE. The CRLB mainly depends on the following parameters:

- The coordinate of the TRPs ($\mathbf{x}_i$)

- The real location of the UEs ($\mathbf{x}$)

- The standard deviation of the TRPs (σ_i).

To find the CRLB, we compute the Fisher Information Matrix (FIM) first [23], whose elements are defined as

$$[\mathbf{I}(\mathbf{x})]_{ij} = -\mathrm{E}\left[\frac{\partial^2 \ln P(\hat{\mathbf{d}}|\mathbf{x})}{\partial \mathbf{x}_i \partial \mathbf{x}_j}\right]. \tag{7.29}$$

Then, we use the PDF given in (7.12), the FIM of the TDOA MLE is calculated as

$$\mathbf{I}(\mathbf{x}) = \begin{bmatrix} \sum_{\substack{i,j=1,\ldots,N \\ i>j}} \frac{A_{ij}^2(x)+B_{ij}\tilde{d}_{ij}}{\sigma_i^2+\sigma_j^2} & \sum_{\substack{i,j=1,\ldots,N \\ i>j}} \frac{A_{ij}(x)A_{ij}(y)}{\sigma_i^2+\sigma_j^2} \\ \sum_{\substack{i,j=1,\ldots,N \\ i>j}} \frac{A_{ij}(x)A_{ij}(y)}{\sigma_i^2+\sigma_j^2} & \sum_{\substack{i,j=1,\ldots,N \\ i>j}} \frac{A_{ij}^2(y)+B_{ij}\tilde{d}_{ij}}{\sigma_i^2+\sigma_j^2} \end{bmatrix}, \tag{7.30}$$

where $A_{ij}(x)$ and $A_{ij}(y)$ are the partial derivatives of $\tilde{d}_{ij}$ over x and y respectively, $A_{ij}(x)$ can be expressed as (7.31). $A_{ij}(y)$ can be obtained by the same equation by replacing x as y:

$$A_{ij}(x) = \frac{\partial}{\partial x}\tilde{d}_{ij}(x) = \frac{2(x-x_i)}{d_i} - \frac{2(x-x_j)}{d_j}. \tag{7.31}$$

B_{ij} is the second order partial derivatives of $\tilde{d}_{ij}$ over x or y. B_{ij} is a constant which can be expressed as

$$B_{ij} = \frac{\partial^2 \tilde{d}_{ij}(x)}{\partial x^2} = \frac{\partial^2 \tilde{d}_{ij}(y)}{\partial y^2} = \frac{2}{d_i} - \frac{2}{d_j}. \tag{7.32}$$

Then, the (1,1) and (2,2) elements of the $\mathbf{I}^{-1}$ are the CRLB of the $\hat{x}$ and $\hat{y}$, denoted as B_x and B_y respectively. The joint CRLB is the given by $B_x + B_y$.
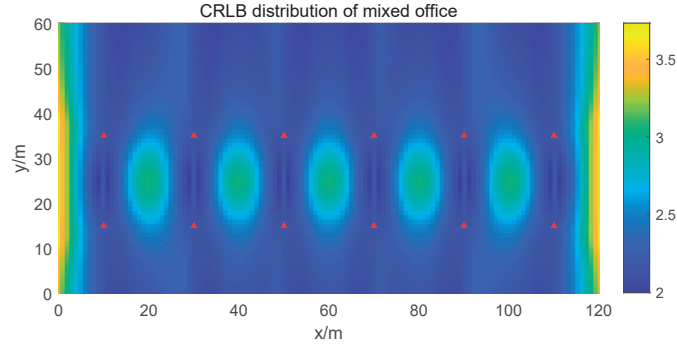
Figure 7.2: Theoretical CRLB distribution in Mixed office environment, $\sigma_{\text{TOA}} * c = 3.3$ m. The colour bar is in the unit meter.

In the NLOS environment, like in the mixed office, the NLOS probability can reach 23%. If an ideal detector can remove all the NLOS TRPs, the measurement can achieve the CRLB. Accordingly, in a simulated environment, when calculating the CRLB, the TDOA estimate from NLOS TRP is removed. Fig. 7.2 is the distribution of the CRLB in the mixed office. The standard deviation of the noise of each TRPs times the speed of light is assumed to be 3.3 m.

Form the figure, one can observe that the location error is large in the middle of each four TRPs and on the edge of the wall. The lower bound of the UE location error varies from 1.8 m to 3.8 m, depending on the location of the UEs.

7.4 NLOS Solutions

In the indoor office, it is frequent that the LOS path between the UE and the TRP is obstructed. In the two scenarios of interest, the mixed office has 23%, and the open office has a 10% probability of being NLOS.

Mathematically, in the TOA measurement model (7.1), the b_i term is non-zero. The NLOS link may seriously degrade the positioning accuracy. An ideal solution is to identify the NLOS TRPs and remove them from the measurement group. The final estimation would only be determined by the left TRPs. However, in practice, this method always has the possibility of the wrong estimation. The section mainly introduces the methods, RWGH and Residual Testing (RT), and analyzes the problem in practice.

7.4.1 Residual Weighting Algorithm

In the NLS method, the weight of each link is equal. If one or more TRP is an NLOS TRP, the NLS's final result may be biased. RWGH [22] is a method to mitigate this effect by searching for all the possible combinations selected from a total of N TRPs.

44

After that, it gives each combination a weight based on the residual squared error.

First of all, RWGH starts with listing all the combinations and computing the estimated UE location by the corresponding combination. The number of combinations N_{cb} in a N TRPs system is given by (7.33). The combinations contain 3 to N TRPs selected from a total of N TRPs.

$$N_{cb} = \sum_{i=3}^{N} \mathrm{C}_i^N, \tag{7.33}$$

where C is the combination operator given by $\mathrm{C}_i^n = \frac{n!}{(n-i)!\,i!}$.

Recalling the detection criterion in (7.25), the final UE location $\hat{\mathbf{x}}$ is the estimate that minimizes the sum of the residual square over all data sets. For convenience, The estimation for the k-th combination is denoted as $\hat{\mathbf{x}}(k)$ and the sum of the residual squares of $\hat{\mathbf{x}}(k)$ over measurement set S is denoted as $R_{es}(k)$. In the LS solution, the residual $R_{es}(k)$ is the indicator showing which estimate is the best. The best estimate $\hat{\mathbf{x}}$ has the minimum residual which,

$$R_{es}(k) = \sum_{\substack{i,j \in S \\ i \neq j}} [\hat{d}_{ij} - (\|\hat{\mathbf{x}}(k) - \mathbf{x}_i\| - \|\hat{\mathbf{x}}(k) - \mathbf{x}_j\|)]^2,$$
$$S = \{S_k \mid k = 1, 2, ..., N_{cb}\}, \tag{7.34}$$

where $\hat{d}_{ij}$ is the TDOA multiplied by the speed of light, the $\mathbf{x}_i$ and $\mathbf{x}_j$ represent the i-th and the j-th TRP coordinates.

Commonly, when an NLOS TDOA measurement is in the data sets, the residual of the estimation is likely greater than when all of the measures are LOS. A small example can illustrate this phenomenon. In Fig. 7.1, the probability density function given by each TDOA measurement is a hyperbolic line. If all the TRPs are LOS, five hyperbolic lines would likely be intersected on one single point. The intersection point is the final measurement. The sum of the shortest distance between this point and the hyperbolic line can be regarded as the residual. In such a case, the residual is not large because all the hyperbolic lines are not far from the point. However, when one of the TDOA measurement is NLOS, the related hyperbolic line would deviate from that point. The difference between them results in a larger residual than the one in all LOS TRPs case.

Overall, there are N_{cb} combination sets of estimation and the corresponding residual. Since all of the sets are commutative constructed, some of the sets contain no NLOS measurements or less NLOS measurements than the others. If the final result can rely more on the estimate computed from the set with all LOS TRPs, the NLOS effect can be reduced. This is the main idea of the RWGH which evaluate the weight for each estimate by the residual. However, different residual contains different terms in the polynomial. A wise way is to remove the dependence from the set size is normalizing the residual by:

$$\tilde{R}_{\text{es}}(\hat{\mathbf{x}}, S) = \frac{R_{\text{es}}(\hat{\mathbf{x}}, S)}{C_2^i},\tag{7.35}$$

where i is the number of TRPs in the combination S.

The final estimate is given by calculating the linear weighted average of all the intermediate estimates $\hat{\mathbf{x}}(k)$. The weight for each $\hat{\mathbf{x}}(k)$ is the reciprocal of the normalized residual, as:

$$\hat{\mathbf{x}}_{\text{final}} = \frac{\sum_{k=1}^{N_{cb}} \hat{\mathbf{x}}(k) \, [\tilde{R}_{\text{es}}(\hat{\mathbf{x}}(k), S_k)]^{-1}}{\sum_{k=1}^{N_{cb}} [\tilde{R}_{\text{es}}(\hat{\mathbf{x}}(k), S_k)]^{-1}}.\tag{7.36}$$

7.4.2 NLOS-TRP identification

Another way to mitigate the NLOS effect is by identifying the NLOS TRPs from the group. If all the NLOS TRPs can be found and removed correctly, the final result would be significantly improved. [26] proposes a method that identifies the number of LOS TRPs (called Dimension). The dimension estimates by a technique called Residual Testing (RT) which compares the residuals from all the combinations against a predetermined Threshold (TH). If only a small amount of residuals, say 10% of the total, are above TH, all the TRPs are LOS. Otherwise, there are one or more NLOS TRPs in the group.

In the thesis work, a new method that combines the idea of the RT and the RWGH is proposed. The evaluation result is given in Chapter 8, which shows that the combined method provides a more reliable result than only using RWGH. Besides, the flow chart of this proposed algorithm is given in Subsection 7.4.3.

In this section, an N-TRP positioning system is applied. The RT begins with a procedure similar to what RWGH does by listing N_{cb} combinations and calculating the corresponding N_{cb} estimates. After then, the final result given by RWGH is regarded as the reference denoted as $\hat{\mathbf{x}}_{\text{ref}}$. The reference estimate is used to calculate the normalized residuals. A square of the normalized residuals for x and y coordinates are given by

$$\begin{aligned}
\chi_x^2(k) &= \frac{[\hat{x}(k) - x_{\text{ref}}]^2}{B_x(k)} \\
\chi_y^2(k) &= \frac{[\hat{y}(k) - y_{\text{ref}}]^2}{B_y(k)} \ , \ k = 1, 2, ..., N_{cb},
\end{aligned}\tag{7.37}$$

where the $\chi_x^2(k)$ and $\chi_x^2(k)$ are the squared residual error of the x and y coordinates follows chi-square distribution in LOS cases, the x_{ref} and y_{ref} are the first and second elements in $\hat{\mathbf{x}}_{\text{ref}}$ given by RWGH, which is the most reliable estimate among all the estimates $\hat{\mathbf{x}}$, $B_x(k)$ and $B_y(k)$ are the CRLB in the estimated UE location $(\hat{x}(k), \hat{y}(k))$

which can be obtained from the (1,1) and (2,2) elements of the inverse of the Fisher information matrix, as (7.30).

Theoretically, in a case with all LOS TRPs and infinitive SNR, the normalized residual χ_x and χ_y have a $N(0,1)$ PDF. Consequently, the square of them in (7.37) follows a central Chi-square distribution with one degree of freedom. If one or more TRPs are NLOS, the residual values in (7.37) follow the non-central Chi-square distribution.

An example showing how to determine whether one or more TRP is NLOS is given in Fig. 7.3. In Fig. 7.3, the left subfigure is measured in a LOS environment, and the right one is in the NLOS environment. The blue curve gives the theoretical PDF of the right tail area of the chi-square distribution. The histogram of the residual is plot in the same figure for comparison with the blue curve. One of the ways to define the criterion is by checking how many normalized residuals $\chi_x^2(k)$ and $\chi_y^2(k)$ are higher than the threshold, say 2.72 in here. The residuals that are above the threshold are called 'outliers'. From the theoretical central distribution curve, if the number of the outliers is less than the TH 2.72, the distribution is regarded as a central Chi-square distribution. Otherwise, it is a non-central distribution.
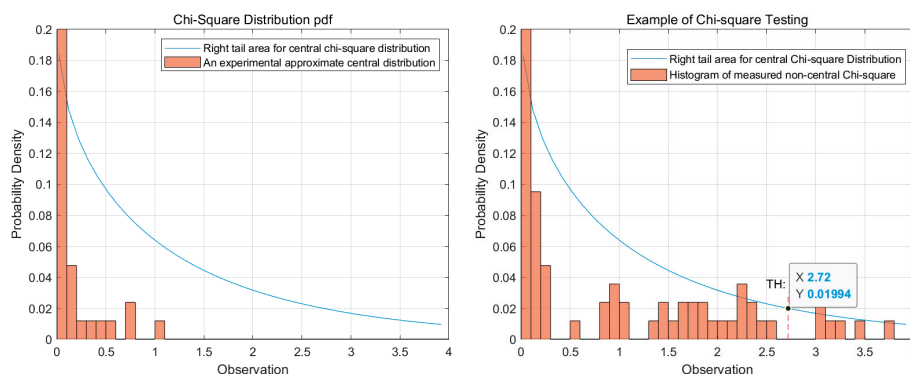
Figure 7.3: Examples of the histograms of experimental normalized residuals $\chi_x^2(k)$ and $\chi_y^2(k)$. The left figure is under LOS case and the right one is under NLOS case. The theoretical PDF of the right tail area of chi-square distribution is given by the blue curve for comparison.

Nevertheless, in the realistic case, the amount of the total residual value is not enough. In a 6 TRPs system, only 84 residual values can be used to test. In the algorithm, a specified percentage of the total combinations would be considered as the outliers. The percentage can not be tiny. For example, $2\% \times 82$ is a tiny number that may not cover all the combinations with NLOS. A recommended percentage, 10%, is proposed in [26].

If more than 10% of the residuals are above the threshold, it means at least one NLOS TRP is in the group. The next step is to identify the one that is the most likely the NLOS TRPs. Identification starts with extracting the indexes of the outliers and finding the corresponding combinations denoted as $S' = \{S'_i \mid i = 1, ..., N_{ol}\}$. Then, the algorithm find out the one TRP that appears the most frequently in S'

and regard this TRP as the NLOS TRP. The NLOS TRP would be removed from the group afterword. The UE estimate would be recalcualted only by the five left TRP. This method can be expended to search for the second or the third NLOS TRPs. The second and the third NLOS TRP detection should be more cautious because the χ^2 values are much less than in the first detection. The histograms of the χ^2 in the second or third detection would be more discrete, making the detection unreliable.

7.4.3 Flow chart for RWGH+RT method
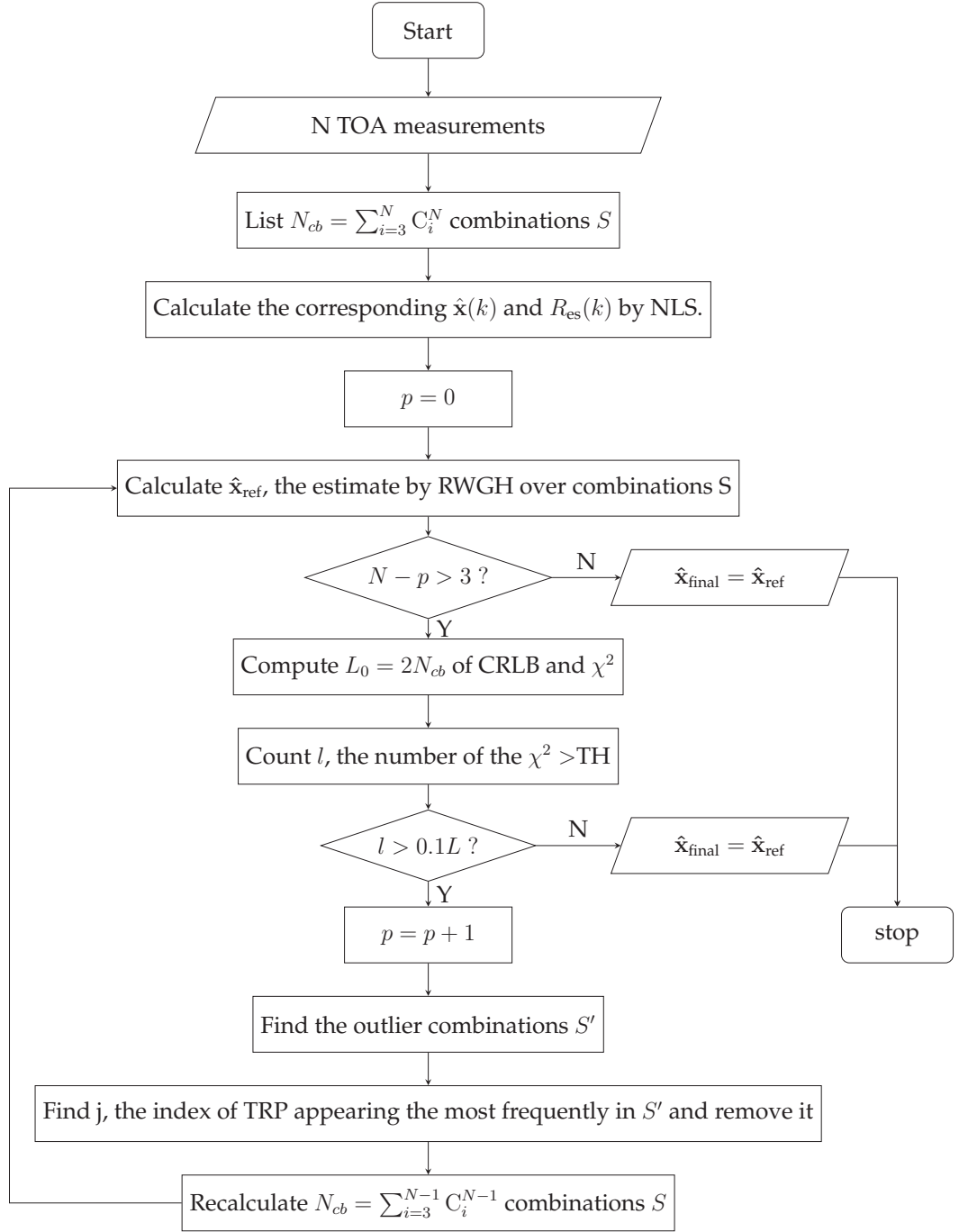
7.4.4 Geometry Constrain by AoD

According to the study on the NLOS channel cluster model, the first path in the CIR may not reflect the LOS path in reality. From the detection aspect, this may result in a larger TOA measurement than the real value. The AoD measurement in NLOS cases can be completely random. Since the AoD measurement is more sensitive than the TOA in our eight elements Multiple Input Multiple Output (MIMO) system, using the AoD measurement to refine UE location becomes very hard.

A way to utilize the AoD information is by setting up a constraint in the iteration step in the non-linear least square method. In Fig. 7.4, six sectors with a certain radian are derived from the six corresponding TRPs. The union of them, the yellow colour region, is the available region for the estimated UE location.
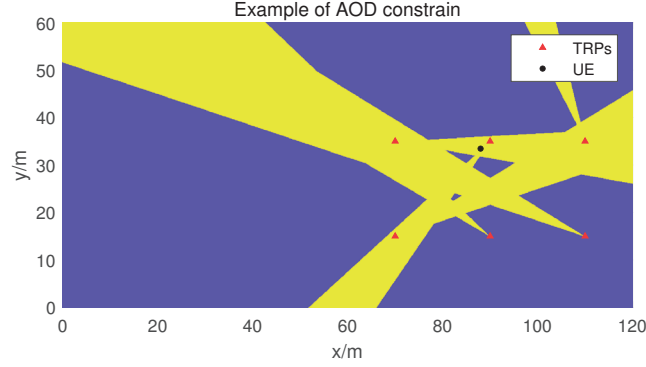
Figure 7.4: An example of geometry constrain by measured AoD, the width of each sector is $16°$. The yellow region is the constrain $\mathbf{C}$ for the estimated UE location $\hat{\mathbf{x}}$, $\hat{\mathbf{x}} \in \mathbf{C}$.

As a result of this, we define the probability that the UE is within an x radian as P_x. The probability of UE is within the union of six sectors denotes as P_{union} which is the function of the P_x:

$$P_{\text{union}} = 1 - (1 - P_x)^6. \tag{7.38}$$

If one wants to make sure that 90% of the UEs can follow the constrain, the corresponding P_x is 32%. Having the probability P_x, the radian x can be obtained by the Cumulative Distribution Function (CDF) of the nAoD, which will be discussed in the result part.

7.5 Hybrid TDOA+AoD Algorithm

The AoD obtained from the UE side can be used to improve accuracy. In this section, AoD non-linear least square methods are first introduced. After then, two hybrid TDOA+AoD localization algorithms would be proposed. The first algorithm is by maximum likelihood method, which aims to obtain the highest accuracy. The second one is by linear least square method aiming to reduce the computational complexity.

7.5.1 AoD ML algorithms

Similar to the TDOA ML algorithm, the AoD ML is by searching for the best estimate that can maximize the joint conditional probability as in (7.39). The ML equation can be transferred into an LS equation. The equivalent LS method is by minimizing the weighted and squared residual. Here the weight for each squared residual is the reciprocal of the AoD variance:

$$
\begin{aligned}
\hat{\mathbf{x}} &= \arg\max_{\mathbf{x} \epsilon \mathbf{C}} \left\{ \prod_{i=1}^{N} \frac{1}{\sqrt{2\pi}\sigma_{\text{AOD}_i}} \exp\left[-\frac{(\hat{\phi}_i - \tilde{\phi}_i)^2}{\sigma_{\text{AOD}_i}^2} \right] \right\} \\
&= \arg\min_{\mathbf{x} \epsilon \mathbf{C}} \left\{ \sum_{i=1}^{N} \frac{(\hat{\phi}_i - \tilde{\phi}_i)^2}{\sigma_{\text{AOD}_i}^2} \right\}.
\end{aligned}
\tag{7.39}
$$

The $\tilde{\phi}_i$ can be calculated in terms of the hypothesis UE location and the TRP location, which

$$
\tilde{\phi}_i = \frac{y - y_i}{|y - y_i|} \arccos(\frac{x - x_i}{r_i}),
\tag{7.40}
$$

where the output from the inverse trigonometric function $\arccos$ is in the range (0,180).

We plot the probability density distribution map in Fig. 7.5 to visualize the effect from each TRPs. Each of the AoD measurements can constrain the UE locations into a sector emitted from the corresponding TRPs. The cross-section of the six sectors is regarded as the most probable UE location.

7.5.2 ML Hybrid TDOA+AoD Algorithm

In the indoor office scenario, each TRP equips with a MIMO antenna, which makes the AoD measurement possible. However, using the AoD measurement to refine the location estimated from TDOA is still a challenge.

The thesis work proposed a maximum likelihood algorithm for hybrid TDOA+AoD is given by (7.41). This method derives from the assumption that the error of the
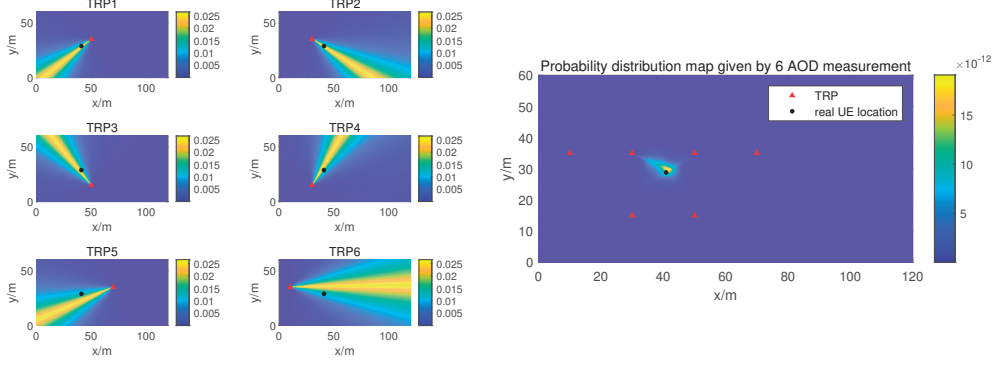
Figure 7.5: Left figure is an example of a probability density distribution map given by the AoD ML from the N-th TRP. The joint probability of the 6 PDF distribution maps for AoD ML is the right figure. The standard deviation of the AoD measurement is set to $15°$.

measured TOA and AoD follow a normal distribution with zero means. The final probability is contributed by TDOA and AoD equally. The objective of the algorithm is to find the best estimate that can maximize the joint likelihood.

$$\hat{\mathbf{x}} = \arg\max_{\mathbf{x}\in\mathbf{C}} \prod_{\substack{i,j=1,\ldots,N \\ i>j}} \frac{1}{\sqrt{2\pi}\sigma_{\text{TDOA}_{i,j}}} \exp\left(-\frac{(\hat{d}_{ij}-\tilde{d}_{ij})^2}{\sigma_{\text{TDOA}_{i,j}}^2 * c^2}\right) \times$$

$$\prod_{i=1}^{N} \frac{1}{\sqrt{2\pi}\sigma_{\text{AoD}_i}} \exp\left(-\frac{(\hat{\phi}_i-\tilde{\phi}_i)^2}{\sigma_{\text{AoD}_i}^2}\right) \tag{7.41}$$

$$= \arg\min_{\mathbf{x}\in\mathbf{C}} \left\{ \sum_{\substack{i,j=1,\ldots,N \\ i>j}} \frac{(\hat{d}_{ij}-\tilde{d}_{ij})^2}{\sigma_{\text{TDOA}_{i,j}}^2 c^2} + \sum_{i=1}^{N} \frac{(\hat{\phi}_i-\tilde{\phi}_i)^2}{\sigma_{\text{AoD}_i}^2} \right\},$$

where $\sigma_{\text{TDOA}_{i,j}}$ is the standard deviation of the $\text{TDOA}_{i,j}$, which is equal to $\sigma_{\text{TOA}_i} + \sigma_{\text{TOA}_j}$

7.5.3 Linear LS Hybrid TDOA+AoD Algorithm

[24] proposes a linear least-square solution. Firstly, this method assumes that the noise of the measured AoD is small so that by Taylor expansion, the AoD noise can be transferred into a linear form, as in (7.42). Note that, the AoD noise here is in the unit meter, which is a function of AoD error and the distance d.

$$N_{\text{AOD},i} = d_i \sin(n_\varphi)$$
$$\approx d_i n_\varphi \ , \ \text{when } n_\phi \ll 1, \tag{7.42}$$

where N_{AOD} is the estimate error in unit meter, n_φ is the AOD estimate error.

After that, a cost function with the AoD term is derived, which is similar to the (7.26). The final estimated location can be calculated by (7.28).

The hybrid TDOA+AoD residual vector can be calculated by (7.26), but the $\mathbf{h}$ and $\mathbf{G}_a$ expanded to

$$
\mathbf{h} = \begin{bmatrix} d_{2,1}^2 - K_2 + K_1 \\ d_{3,1}^2 - K_3 + K_1 \\ \vdots \\ d_{N,1}^2 - K_N + K_1 \\ -2x_1 \sin\phi_1 + 2y_1 \cos\phi_1 \\ \vdots \\ -2x_N \sin\phi_N + 2y_N \cos\phi_N \end{bmatrix} , \quad \mathbf{G}_a = - \begin{bmatrix} x_{2,1} & y_{2,1} & d_{2,1} \\ x_{3,1} & y_{3,1} & d_{3,1} \\ \vdots & \vdots & \vdots \\ x_{N,1} & y_{N,1} & d_{N,1} \\ -\sin\phi_1 & \cos\phi_1 & 0 \\ \vdots & \vdots & \vdots \\ -\sin\phi_N & \cos\phi_N & 0 \end{bmatrix} , \qquad (7.43)
$$

where the ϕ_i is the AoD measurement from the i-th TRP.

8 Simulation Results

This chapter is divided into five sections: The first one is an investigation on statistical channel properties. Then, the second section is the simulation results of the TOA and AoD estimator. After that, the third section is the evaluation of the linear localization algorithms. In the last two parts, the investigation and evaluation of the results from NLOS mitigation solutions and AoD-based solutions are given. In DL-positioning, UE estimates the TOA and AOD, and report these measurements to the location server. After that, the location server implements the localization algorithms.

All the simulations are implemented in the indoor office environment. The number of used gNB is six. The positioning error mainly evaluates by the CDF of the estimated horizontal location errors from 1000 UEs.

8.1 Statistical Channel Properties

The PDF of SNR is given in Fig. 8.1 which is measured from 6000 simulated received PRS. The SNR level, in reality, depends on the distance between TRP and UE r_i and the shadow fading σ_{SF}^2.
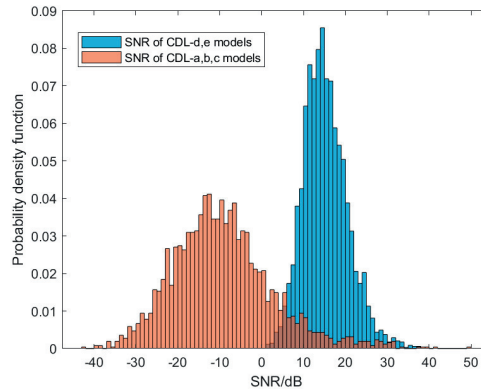
Figure 8.1: The probability density distributions of the received signal SNR under LOS model (CDL-D, E) and the NLOS model (CDL-A, B, C), 6000 measurements.

The orange histogram is the PDF of the SNR measured from the CDL-A, B, and C model which are the NLOS models. The average SNR is about -10 dB, and the standard deviation of it is 10 dB. The blue histogram is the PDF from the CDL-D, E model, which are the LOS models. The SNRs from the LOS channels are better than the NLOS channels, which have 18 dB on average and 5 dB standard deviation.

One can observe that the LOS TRP can receive 28 dB more power than the NLOS TRP. The NLOS has 5dB larger shadow fading than the LOS channel. From the positioning point of view, larger power means higher accuracy in TOA detection. However, it is hard to distinguish the LOS and the NLOS TRP only from the SNR. From the figure, the mutual area occupies about 20% and 15% area of the NLOS PDF and LOS PDF. Moreover, the estimated SNR would not be 100 per cent correct. Due to these two reasons, it is hard to tell whether a TOA measurement is good or not by the SNR of the received signal.

Another parameter to evaluate the TOA detector accuracy is the standard deviation of the noise of TOA. The noise of TOA denotes as n_{TOA} and which can be modeled as $b_i + n_i$ in the (7.1). The $\sigma_{n_{\text{TOA}}}$ is the normal distributed with zero mean. By applying different thresholds, the detected TOA would not be the same. From the (6.11), the threshold is affected by the β. The standard deviation of the n_{TOA} as a function of β is given in Fig. 8.2. From the figure, one can conclude that, if the β is 0.1, the standard deviation of n_{TOA} in mixed office is 2.7 $\times 10^{-8}$ s and the one in the open office is 2.2 $\times 10^{-8}$ s.
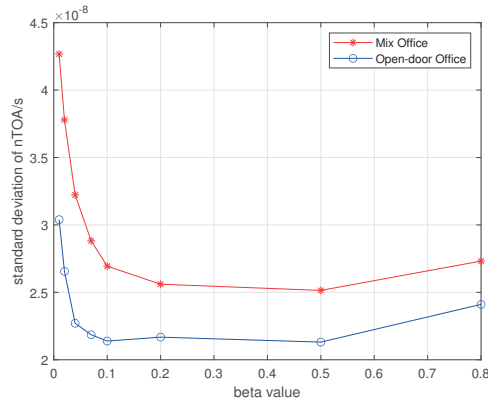
Figure 8.2: The standard deviation of the TOA measurement noise as a function of the β.

Having a similar definition with n_{TOA}, AoD noise (n_{AOD}) is the error in the measured angle of departure using the proposed method introduced in Chapter 6. The CDF of the AoD noise in three scenarios are given in Fig. 8.3. In the ideal cases, with all LOS TRPs, 80% of the UEs can have less than 0.4° of error in AoD. However, the AoD measurement is affected by the NLOS link in the office environment. In the mixed and the open door offices, 80% UE would have up to 48° n_{TOA}.
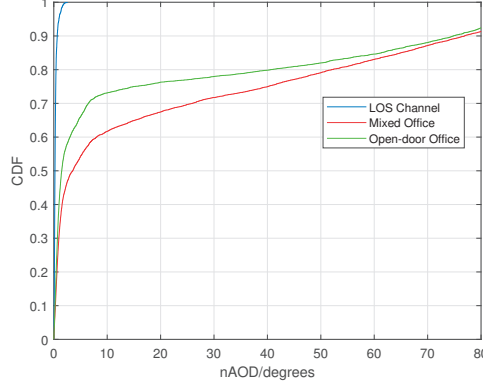
Figure 8.3: The CDF of the Angle of departure noise in Mixed office and Open office environment.

8.2 Evaluation of the TOA Estimator

In this section, some properties of the TOA estimator and the corresponding localization algorithm are further investigated. Some setting in these two-part are still variables. This section aims to find out the best setting to match up the indoor office scenario.

8.2.1 Evaluation of Beam Selection Methods

As mentioned in Table 6.1, eight different ways to qualify the beam is proposed. Fig. 8.4 presents a comparison among them. The results are measured from 1000 UEs in a mixed office. The used localization algorithm is TDOA NLS method. The evaluated results are from the following beam selection criterion:

- Scheme 1: 'TOA1': the beam with the shortest TOA estimate which satisfies $|\text{TOA} - \overline{\text{TOA}}| < 2\sigma_{\text{TOA}}$.

- Scheme 2: 'TOA2': the beam with the shortest TOA estimate which satisfies $|\text{TOA} - \overline{\text{TOA}}| < 10\sigma_{\text{TOA}}$.

- Scheme 3: 'SNR': the beam with the largest estimated SNRs given by $\overline{\Lambda_l(\tau)} / N_f$.

- Scheme 4: 'MPAR': the beam with the largest main peak to average ratio: $1 / \overline{\Lambda_l(\tau)}$.

- Scheme 5: 'MPMR': the beam with the largest main peak to median ratio: $1 / \text{median}(\Lambda_l(\tau))$.

- Scheme 6: 'FPAR': the beam with the largest first peak to average ratio: $\Lambda_l(\tau_{\text{FP}}) / \overline{\Lambda_l(\tau)}$.

- Scheme 7: 'FPMR': the beam with the largest first peak to median ratio: $\Lambda_l(\tau_{\mathrm{FP}}) / \mathrm{median}(\Lambda_l(\tau))$.

- Scheme 8: 'RSRP': the average of the signal power over a symbol.
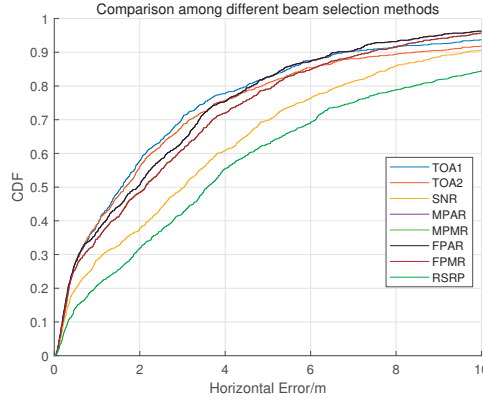
Figure 8.4: Comparison among 8 different ways of beam selection.

From the figure, one can observe that only 6 curves show up because of the overlap between MPAR and MPMR, and the overlap between FPAR and FPMR. It means that the average and the median have no difference. One can also observe that three methods, the 'TOA1', 'TOA2', and 'FPAR', have a decent positioning accuracy. The 'TOA1' method has the best performance among them.

8.2.2 Evaluation of the impact of the threshold

From the study in Chapter 6, in the adaptive threshold peak detector, the estimated LOS path was given by the first peak that was above the threshold. In most of the LOS channels, the LOS path is the largest peak in the CIR. The σ_{nTOA} in LOS channel is about 10^{-9} s which only provide 0.3 m error in the range difference $d_{i,j}$. However, in the NLOS channel, the main peak is no longer the LOS path. The LOS path is usually several nanoseconds ahead of the main path and its amplitude and phase are unknown. The thesis work investigates the ratio between the amplitude of the LOS path and the main path to determine a proper threshold.

Fig. 8.5 is the amplitude distribution of the LOS path in the normalized CIR measured in the mixed office environment, which denotes as β_r. β_r can be given by

$$\beta_r = \Lambda\left(\frac{r}{c}f_{\mathrm{samp}}\right) - N_f,\tag{8.1}$$

where the Λ is the normalized CIR, N_f is the estimated noise figure and f_{samp} is the sampling frequency.

Figure 8.5: The probability density distribution and the cumulative distribution of the amplitude of the LOS path in the normalized measured CIR, simulating 3000 UEs.

The β is a factor in the (6.11). In here, if β_r is smaller than β, the LOS would be filtered out. When the β_r is 1, it means that the LOS path is the maximum peak in the CIR. The LOS path in 33% of the links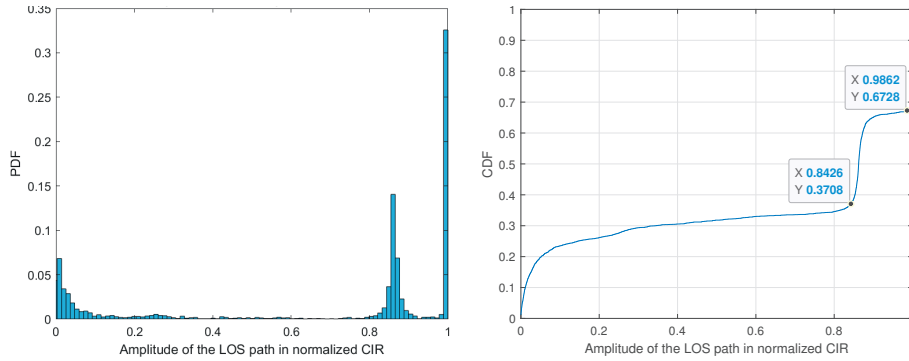 is the maximum peak, which can be ideally detected by the TOA estimator. 30% of the amplitudes are around 0.84, and 25% of the amplitudes are below 0.1. Based on these, we can conclude that if the β is 0.84, at least 63% of the TOA can be correctly detected. For the rest of the link, the LOS path can be captured by lowering the β. However, if the β is set to an extremely low value, the estimator would select a peak even lower than the LOS path. The noise in the PRS signal may create this type of peak. Practically, this 'noise path' is randomly distributed and can be anywhere in the CIR. Once the 'noise path' is regarded as the LOS path by mistake, the error brings from that is unpredictable.

From the measurement perspective, we want the noise of the estimated TOA can be lower than a level, say 10^{-8} s, which can transfer into 3m distance estimate error. For convenience, the TOA estimates with more than 10^{-8} s error from the real value are called 'bad estimate'. As a result of this, two behaviours happened in the NLOS channel that causes the wrong estimate defines as follow:

- Overestimation: the threshold filter out the real LOS path. The delayed path above the threshold is selected. The nTOA $> 10^{-8}$ s.

- Underestimation: the threshold is too low to filler out the 'noise path'. The 'noise path' ahead of the LOS path is selected. The nTOA $< -10^{-8}$ s.

Fig. 8.6 are the probability of the overestimation and underestimation as a function of the threshold. These two plots were measured under a mixed office and open office environment. One can observe that the probability of the overestimation is increased by β. On the opposite, the underestimation probability decreased to β. How to set up the threshold become a trade-off problem. In the thesis work, β is set to 0.1, which has the lowest probability of misestimation.
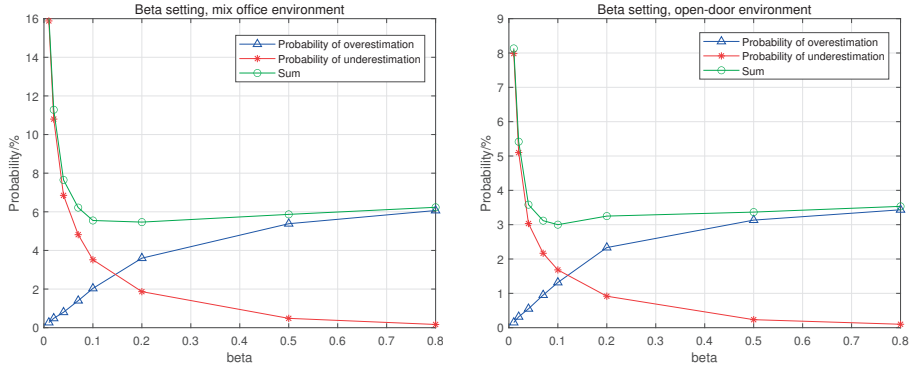
Figure 8.6: The probability of underestimation and overestimation of the first path versus the β in Mixed office and Open office, the sum of them is shown in the green line.

8.3 Evaluation of the linear localization algorithms in office environment

In Chapter 7, four different linear algorithms are introduced, which are AML, Chan's, AOD linear LS, and Hybrid TDOA+AoD algorithms. The linear algorithms are the approximate approach of the non-linear version. The accuracy of it is not as high as the non-linear algorithm. The advantage of them is the low computational complexity. An evaluation of the location accuracy of the linear algorithms is given in Fig. 8.7.

Additionally, to investigate the performance difference between linear algorithms and non-linear algorithms, the result given by TDOA non-linear least square method is regarded as a reference shown in the green curve in the figure. Table 8.1 is a summary of the performance from these algorithms. The simulation execution time may differ from the programming setup and the computer processor. Therefore, instead of showing the absolute execution times, the thesis work provides the execution time in a unit t_0 to describe the relationships among them.

The algorithms used in the figure are the following:

- Algorithm 1: Hybrid TDOA+AOD linear Least square algorithm(Hybrid).

- Algorithm 2: Chan's algorithm(Chan).

- Algorithm 3: AOD linear least square algorithm (AOD LLS).

- Algorithm 4: AML algorithm(AML).

- Reference algorithm: TDOA non-linear algorithm (TDOA NLS).
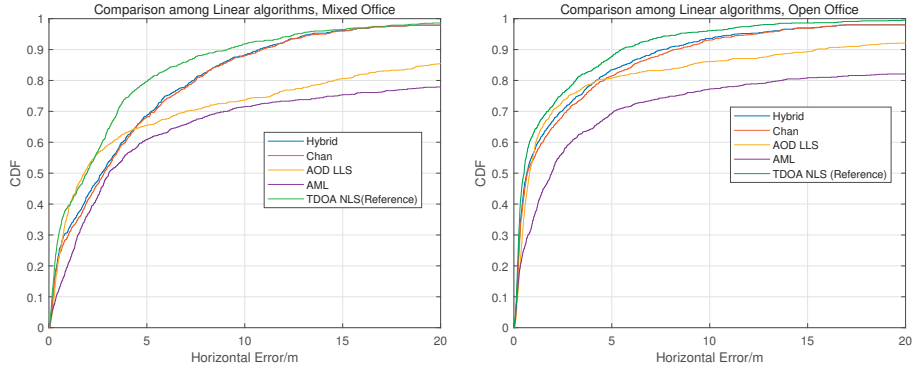
Figure 8.7: Comparison among different linear least squares algorithms in Mixed office and Open office.

Table 8.1: Horizontal errors at CDF = 80% by different linear algorithms.

	Hybrid	Chan	AOD LLS	AML	TDOA NLS
80% Error/m in m.o.	7.447	7.518	14.22	25.34	4.984
80% Error/m in o.o.	4.213	4.628	4.319	13.93	3.154
Execution time in t_0	$2t_0$	t_0	t_0	t_0	$20t_0$

From the figure, one can observe that in the office environment, the hybrid TDOA+ AOD linear LS method has the best positioning accuracy. Using both TDOA and AOD information can improve the accuracy of only using one of them. Nevertheless, improvement is tiny. For the 80% Error, the improvement from Chan's algorithm to the hybrid algorithm is 0.06 m in the mixed office and 0.4 m in an open office. The AML method is the worst one among them in the office environment.

From the comparison of the linear method and the non-linear method, Chan's approach runs approximately 20 times faster than the TDOA NLS method. However, the cost is the accuracy in positioning. If using Chan instead of NLS would reduce 2.5 m and 1.5 m of 80% error in mixed offices and open offices, respectively.

8.4 Investigation and evaluation results of the NLOS mitigation algorithms

8.4.1 The impact of the combinations in RWGH

As described in Section 7.4, in the residual weighting algorithm, all the combinations containing i TRPs are listed in the beginning. The i have to be larger than 3. It is of interest to see which combination distributed the most among them.

Instead of using all the combinations to calculate the final result, the RWGH results from only using the combinations with i TRPs are compared. The RWGH result

from the combination with 6 TRPs (total of TRPs) is the same with NLS methods. Comparisons using the following schemes are given in Fig. 8.8.

- Scheme 1: The RWGH result from the combinations with 3 TRPs.

- Scheme 2: The RWGH result from the combinations with 4 TRPs.

- Scheme 3: The RWGH result from the combinations with 5 TRPs.

- Scheme 4: NLS method (6 TRPs).
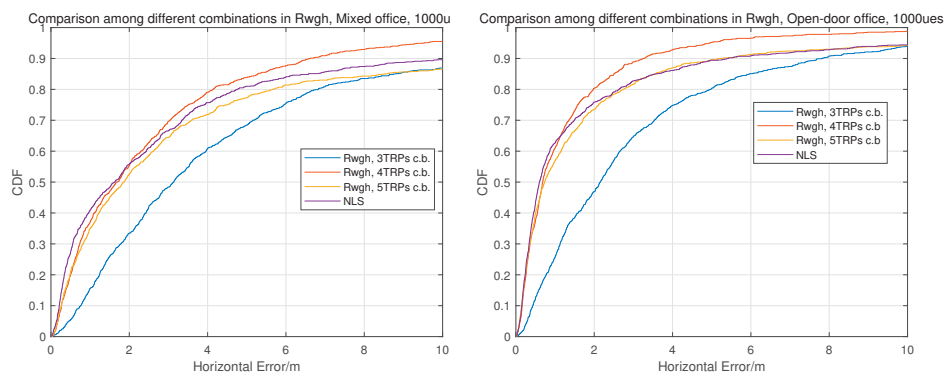
Figure 8.8: Comparisons among the RWGH results using the combinations with 3,4,5 or 6 TRPs. The left plot is measured in Mixed office. The right plot is measured in Open office.

According to the results, the averaging of the combinations with 4 TRPs performs the best positioning results in the indoor office scenario. One of the reasons for that is 4 LOS TRPs + 2 NLOS TRPS are the possible combinations in both the mixed and open office.

8.4.2 The impact of the threshold in RT

Again, the threshold problem is a trade-off problem. In the RT, the threshold plays an important role. If the threshold is too high, some NLOS TRPs may not be detected. On the opposite, if the threshold is too low, some LOS TRPs may be identified as NLOS by mistake. With this, two kinds of behaviors cause the error to define as:

- Overestimation: A case has at least one NLOS TRP, but the RT makes a 'All LOS TRPs' decision. (Ignoring the NLOS TRP).

- Underestimation: A case has at least one NLOS TRP. RT makes a 'Has a NLOS TRP' decision but identify with a wrong TRP. (A LOS TRP is removed by mistake)

The probabilities of these two misestimation behaviors are compared in the Fig. 8.9. The former one is measured under a mixed office. The later one is under the open office.
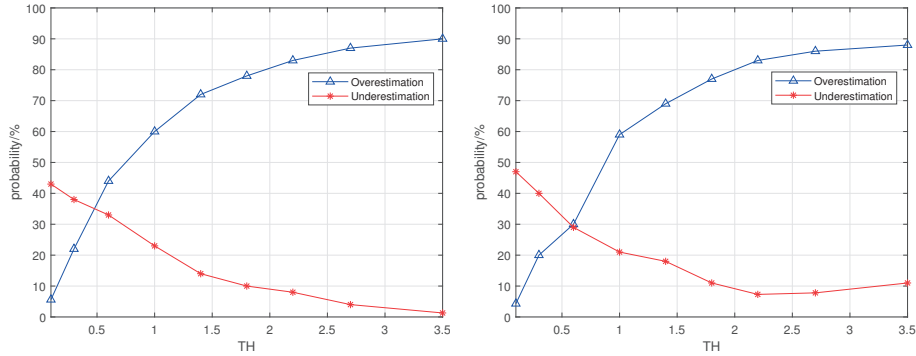
Figure 8.9: The Overestimation rate and the Underestimation rate versus the the Residual testing threshold in Mixed office and Open office environment.

From the figures, we can conclude that more cases with NLOS TRP would be detected if the threshold becomes higher. However, at the same time, the rate of identifying the correct NLOS would be reduced. In other words, if one wants more cases with NLOS TRP can be detected, he has to bear the increasing probability of identifying a LOS TRP as NLOS. From the experiment's point of view, underestimating is more harmful than overestimating in a 6 TRP system. Since the number of measurements is small, if one LOS TRP is removed from the group by mistake, the final result would be biased to the NLOS TOA measurement. On the other hand, if one of the NLOS TRP is ignored, we can maintain the accuracy of the RWGH method.

The final decision is setting the TH to 1.8 to obtain 75% of the overestimation rate and 10% of the underestimation rate. It means that the detector can detect only 25% of cases with at least one NLOS TOA estimate. After that, the detector would identify one TRP as the NLOS TRP, and the possibility of correct identification is 90%.

8.4.3 The impact of number of the NLOS TRPs in RT

In the thesis work, residual testing can detect one NLOS TRP from the group. This method can be extended to enable the detection for the second and third TRP. The following schemes are tested in Fig. 8.10.

- Scheme 1: Enable RT to detect one NLOS TRPs.

- Scheme 2: Enable RT to detect two NLOS TRPs.

- Scheme 3: Enable RT to detect three NLOS TRPs.
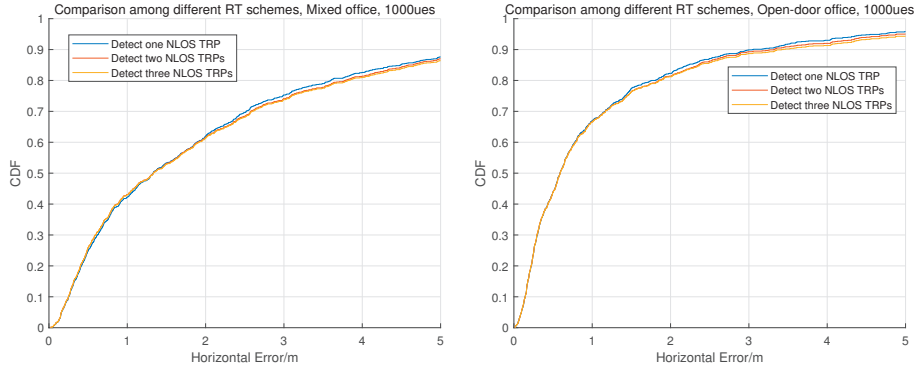
Figure 8.10: The performance of enabling detection for 1, 2 or 3 NLOS TRPs by using residual testing. The left and right plots are measured in Mixed office and Open office respectively.

Observed from the figure, one knows that enabling detection for 2 or 3 NLOS TRPs does not outperform the first scheme. On the contrary, enabling more NLOS TRPs to be detected would lower the performance in our system. One of the reasons is that the probability of wrong identification increases when the total TRPs decreases. In a 6 TRPs system, the second NLOS TRPs identification followed by the removal of the first NLOS TRPs. The number of the available chi-square drops to 32 $(2\sum_{i=1}^{5} C_i^5)$. If the 5 left TRPs to have at least one NLOS TRP, the number of the corresponding outliers should be more than 3. These 3 outliers would determine the final decision of identification, making the decision not as reliable as the first NLOS TRP identification (more than 8 outliers).

If more TRPs are implemented for positioning, the amount of the outliers for NLOS identification would significantly increase. In that system, the identification for the second and the third TRPs would be more reliable.

In the following simulation, the RT algorithm keeps using scheme1, only enabling the first NLOS TRP to be detected to obtain the best performance.

8.4.4 Evaluation of Rwgh and RT methods in the office environment

The performance of the RWGH only and the RWGH+RT methods in the mixed office and the open office are given in Fig. 8.11, respectively. The CDF of the NLS (C_2^6 TDOA) method is regarded as the reference. The compared algorithms are listed by the following:

- Algorithm 1: TDOA Rwgh+RT algorithms.

- Algorithm 2: TDOA Rwgh algorithms.

- Algorithm 3: TDOA NLS.

Table 8.2: Horizontal errors at CDF = 80% by different scheme under NLOS channel.

	RWGH+RT	RWGH	NLS
80% Error/m in m.o.	3.584	4.227	4.808
80% Error/m in o.o.	1.714	1.945	2.606
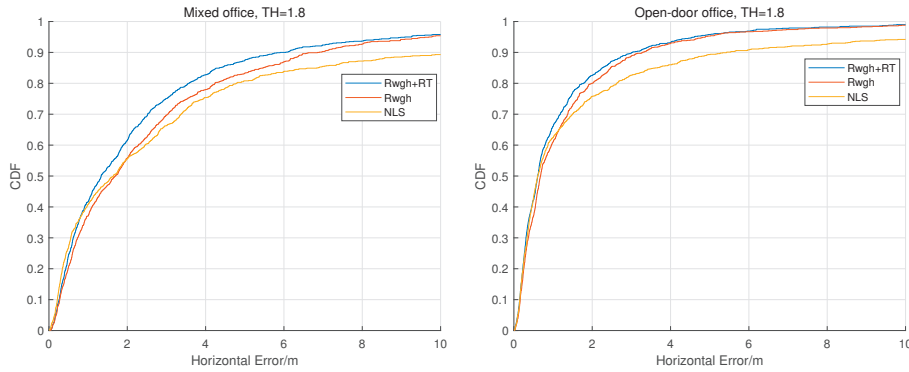
Figure 8.11: Evaluation of Residual weighting and Residual testing methods in Mixed office and Open office. For comparison, the CDF of Non-linear least squares is plot.

From the comparison, one can know that the RWGH and RT algorithm can improve the performance of positioning in either mixed office and open office. The improvement of the 80% error can reach more than 1 meter comparing with the reference.

8.5 Evaluation result of AOD-based algorithms and the hybrid TDOA+AOD algorithms

8.5.1 Evaluation of differet AoD-based localization algorithm under Indoor Office

This section evaluates the AoD-based positioning algorithm. As mentioned before, the thesis proposed a RWGH+RT algorithm to mitigate the NLOS bias in the DL-TDOA method. A similar idea can be applied in the AoD-based algorithm which yields to the RWGH+RT AoD algorithm. Fig. 8.12 is the comprison among these four algorithms, which are

- Algorithm 1: AoD RWGH+RT algorithm.

- Algorithm 2: AoD RWGH algorithm.

- Algorithm 3: AoD NLS algorithm.

- Algorithm 4: AoD Linear LS algorithm.

Table 8.3: Horizontal errors at CDF 80% by different AoD-based algorithms.

	RWGH+RT	RWGH	NLS	LLS
80% Error/m in m.o.	7.375	7.864	10.3	14.8
80% Error/m in o.o.	2.815	3.19	5.196	6.912
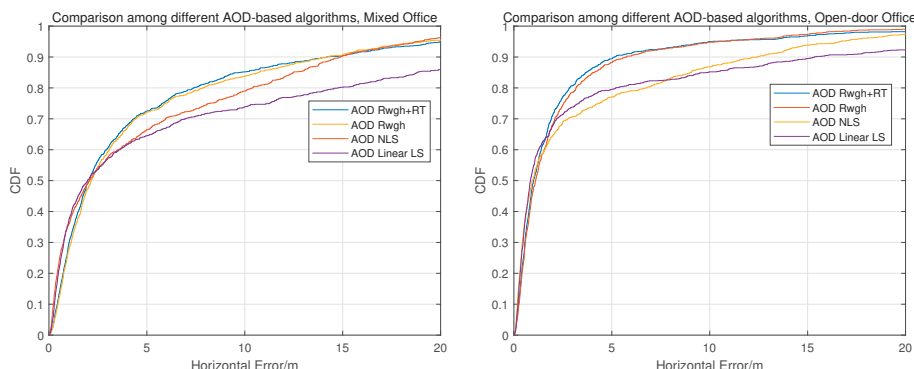
Figure 8.12: Comparison among different AoD-based algorithms under Mixed office and Open office.

From Fig. 8.12, both in mixed office and open office, NLS AoD algorithm and Linear LS AoD algorithm have similar performance, and the results from RWGH AoD algorithm and RWGH+RT AoD algorithm are close. Among these four algorithms, the thesis proposed RWGH+RT AoD algorithm yields the litter better performance than others.

8.5.2 Performance comparison between Hybrid TDOA+AoD ML and Linear LS under Indoor Office

In this part, two hybrid TDOA+AoD algorithms are considered to compare the performances, which are listed below:

- Algorithm 1: Hybrid TDOA+AoD ML algorithm.

- Algorithm 2: Hybrid TDOA+AoD Linear LS algorithm.

As shown in Fig. 8.13, one can observe that the proposed ML hybrid TDOA+AoD performs much better than linear LS hybrid TDOA+AoD algorithm under the indoor office environment. The 80% errors are give in Table 8.4.

8.5.3 Performance Comparison among Hybrid TDOA+AoD based, TDOA-based and AoD-based algorithms

The algorithms under comparison are listed as following:

Table 8.4: Horizontal errors at CDF = 80% by different Hybrid-based algorithms.

	ML Hybrid TDOA+AoD	LLS Hybrid TDOA+AoD
80% Error/m in m.o.	2.914	7.859
80% Error/m in o.o.	1.148	7.513
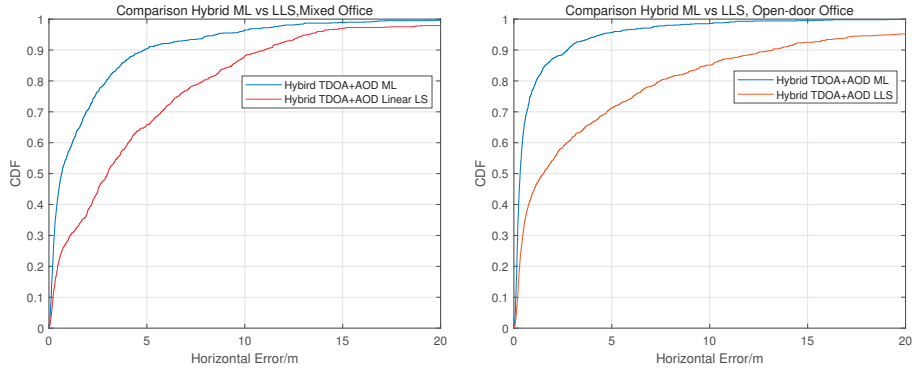
Figure 8.13: Performance comparison between ML Hybrid TDOA+AoD and Linear LS Hybrid TDOA+AoD in Mixed office and open door office environment.

- Algorithm 1: Hybrid TDOA+AoD ML algorithm.

- Algorithm 2: AoD Non-linear least squares algorithm.

- Algorithm 3: Unbiased TDOA Non-linear least squares algorithm.

Fig. 8.14 indicates that the thesis proposed ML hybrid TDOA+AoD algorithm has a better positioning performance than AoD NLS and unbiased NLS TDOA in both open office and mixed office. The 80% error from ML hybrid TDOA+AoD algorithm can is shown in Table 8.5. According to these results, by using the proposed method, the commercial requirement defined in [4] (80% error < 3 meters) can be fulfilled.

Table 8.5: Horizontal errors at CDF = 80% Comparison between ML Hybrid TDOA+AoD, TDOA RWGH+RT and AoD RWGH+RT.

	ML Hybrid TDOA+AoD	TDOA NLS	AoD NLS
80% Error/m in m.o.	2.914	5.055	10.6
80% Error/m in o.o.	1.148	3.109	6.712

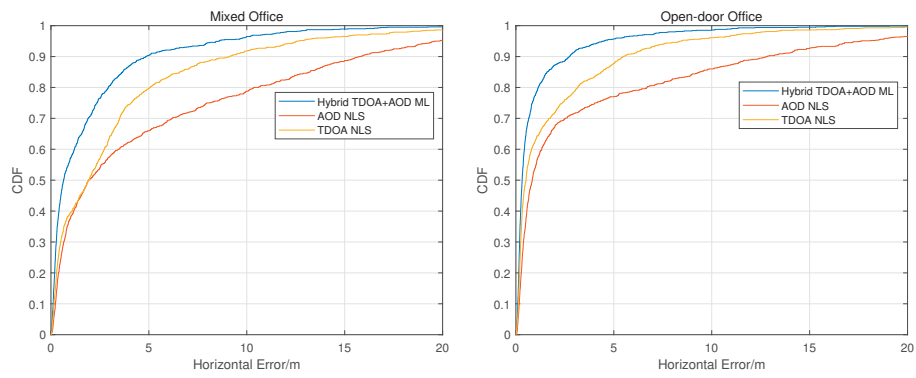**Figure 8.14:** Performance comparison between ML Hybrid TDOA+AoD, NLS AoD and NLS TDOA under Mixed office and Open office environment.

9 Conclusions

In the thesis work, various time and angle related estimation methods and localization algorithms were implemented and evaluated. Some observations can be summarised as follows.

In the initial step, we developed a simulator for indoor office positioning. To validate the simulator setup, we made a comparison between our simulation results and the results reported in [4]. The comparison showed that by using the same receiver, transmitter, and localization algorithm, our simulator could achieve similar performance to Company 1 [11] and Company 2 [12].

For TOA estimation, we implemented the adaptive threshold method [13]. We analyzed the distribution of the amplitude of the LOS path to find the possible threshold value, which could correctly detect TOA in 67% of the cases. Moreover, for studying the remaining cases, the probabilities of two misestimation behaviours were evaluated. The result showed that the estimator could be optimized by setting the beta value to 0.1 in both mixed and open office environments.

In order to achieve a beamforming gain, we implemented the DFT beam sweeping method on the TRP side. Regarding the beam selection part, one of the thesis contributions was using the TOA-based measurements to select the best beam. The results showed that this proposed method could achieve the best performance among all of the tested methods. In the AoD estimation part, we used the least squares method utilizing the beam pattern information. The result showed that the estimator could achieve a low AoD error in LOS cases. However, in an environment with an NLOS link, the average AoD error was 48 $^\circ$.

Based on results from several localization algorithms, the non-linear least squares algorithm showed to outperform all the linear algorithms in both open and mixed office environments. However, the linear algorithms had lower complexity than the non-linear algorithms.

For mitigation of the NLOS effect in OTDOA positioning, we investigated two algorithms, the RWGH [22] and RT [26] algorithms. We merged RWGH and RT method, which improved the positioning performance. To reduce the complexity of the RWGH, we investigated the impact of the combinations. The evaluation showed that the averaging of the combinations with 4 TRPs could achieve the best performance in the office environment. For the RT algorithm [26], we suggested using the estimated UE position from the RWGH algorithm as a reference instead of using the UE estimation from AML algorithm [21]. The RWGH+RT algorithm provided a more reliable residual than in [26]. Also, the evaluation results showed that the RWGH+RT performed better than only using the RWGH algorithm. While investigating the effect of the number of NLOS TRPs, we found that enabling the second and the third NLOS TRP being identified in RT algorithm would not im-

prove the performance in the office environment. The low detection correct rate in the second and third NLOS TRP detection might cause by the lack of the residual. Additionally, we extended the RWGH+RT algorithm to support DL-AoD positioning. The result showed that the RWGH+RT DL-AoD algorithm outperformed other AoD based algorithms.

To combine the TOA and AoD information for positioning, we proposed an algorithm called ML hybrid TDOA+AoD algorithm. In both mixed office and open office environments, this proposed algorithm outperformed linear LS hybrid TDOA+ AoD [24]. By using this technique, the positioning error could achieve 2.9 meters in a mixed office and 1.1 meters in an open office for 80% of UEs. Also, the results could fulfil the commercial positioning requirements as [4] specified (< 3 meters).

For future work, the accuracy could be further improved by combining the hybrid TDOA+AoD method and the RWGH method. However, this is challenging to achieve because as the number of the inputs (TDOA or AoD) increases, the possible combinations increase exponentially. The expansion of the possible combinations would consume more computational capacity in the location server. Due to this reason, some optimization of the algorithm for low complexity can be further investigated.

Bibliography

[1]   Z. Chaloupka. "Technology and Standardization Gaps for High Accuracy Positioning in 5g". In: *IEEE Communications Standards Magazine* 1.1 (2017), pp. 59–65.

[2]   Erik B. L. Dahlman, Johan Sköld and Stefan Parkvall. *5G NR. [Elektronisk resurs] : the next generation wireless access technology.* Academic Press, an imprint of Elsevier, 2018. ISBN: 9780128143230.

[3]   3GPP TS 38.211. *NR; Physical channels and modulation (Release 16).* Technical Specification Group Services and System Aspects 38.211. Version 16.0.0. 3rd Generation Partnership Project (3GPP), Dec. 2019.

[4]   3GPP TS 38.855. *Study on NR positioning support (Release 16).* Technical Specification Group Radio Access Network 38.855. Version 16.0.0. 3rd Generation Partnership Project (3GPP), Mar. 2019.

[5]   3GPP TS 22.261. *Service requirements for the 5G system;Stage 1(Release 17).* Technical Specification Group Services and System Aspects 22.261. Version 17.2.0. 3rd Generation Partnership Project (3GPP), Mar. 2020.

[6]   3GPP TS 38.305. *NG Radio Access Network (NG-RAN); Stage 2 functional specification of User Equipment (UE) positioning in NG-RAN (Release 16).* Technical Specification Group Radio Access Network; 38.305. Version 16.0.0. 3rd Generation Partnership Project (3GPP), Mar. 2020.

[7]   J. A. del Peral-Rosado, R. Raulefs, J. A. López-Salcedo and G. Seco-Granados. "Survey of Cellular Mobile Radio Localization Methods: From 1G to 5G". In: *IEEE Communications Surveys Tutorials* 20.2 (2018), pp. 1124–1148.

[8]   R. Keating, M. Säily, J. Hulkkonen and J. Karjalainen. "Overview of Positioning in 5G New Radio". In: *2019 16th International Symposium on Wireless Communication Systems (ISWCS).* 2019, pp. 320–324.

[9]   Yi Wang, Zhenyu Shi, Yingjie Yu, Su Huang and Lei Chen. "Enabling Angle-based Positioning to 3GPP NR Systems." In: *2019 16th Workshop on Positioning, Navigation and Communications (WPNC), Positioning, Navigation and Communications (WPNC), 2019 16th Workshop on* (2019), pp. 1 –7. ISSN: 978-1-7281-2082-9.

[10]   3GPP TR 38.901. *Study on channel model for frequencies from 0.5 to 100 GHz (Release 16).* Technical Specification Group Radio Access Network; 38.901. Version 16.1.0. 3rd Generation Partnership Project (3GPP), Dec. 2019.

[11]   R1-1902514. "NR Positioning Evaluation Results". Intel Corporation.

[12]   R1-1903021. "Evaluation results for RAT-dependent positioning Techniques". Qualcomm Incorporated.

[13] W. Xu, M. Huang, C. Zhu and A. Dammann. "Maximum likelihood TOA and OTDOA estimation with first arriving path detection for 3GPP LTE system." In: *Transactions on Emerging Telecommunications Technologies* 27.3 (2016), p. 339. ISSN: 21613915.

[14] C. Zhu2 W. Xu1* M. Huang1 and A. Dammann3. "Maximum likelihood TOA and OTDOA estimation with first arriving path detection for 3GPP LTE system". In: *RESEARCH ARTICLE* (2014), p. 18.

[15] J. Wang, Z. Lan, C. Sum, C. Pyo, J. Gao, T. Baykas, A. Rahman, R. Funada, F. Kojima, I. Lakkis, H. Harada and S. Kato. "Beamforming Codebook Design and Performance Evaluation for 60GHz Wideband WPANs". In: *2009 IEEE 70th Vehicular Technology Conference Fall*. 2009, pp. 1–6.

[16] Lie-Liang Yang Du Yang and SO17 1BJ UK Lajos HanzoSchool of ECS University of Southampton. "DFT-based Beamforming Weight-Vector Codebook-Design for Spatially Correlated Channels in theUnitary Precoding Aided Multiuser Downlink". In: *RESEARCH ARTICLE* (2010), p. 4.

[17] Wei Liu and Stephan Weiss. *Wideband Beamforming. [Elektronisk resurs] Concepts and Techniques.* John Wiley Sons, Ltd., 2010. ISBN: 9780470713921.

[18] HiSilicon Huawei. "Performance evaluation for NR positioning". In: *Discussion and Decision* (2019), p. 23.

[19] Yingjie Yu Su Huang Yi Wang Zhenyu Shi and Lei Chen. "Enabling Angle-based Positioning to 3GPP NR Systems". In: *RESEARCH ARTICLE* (2019), p. 7.

[20] I. Guvenc and C. Chong. "A Survey on TOA Based Wireless Localization and NLOS Mitigation Techniques". In: *IEEE Communications Surveys Tutorials* 11.3 (2009), pp. 107–124.

[21] Yiu-Tong Chan, H. Yau Chin Hang and Pak-chung Ching. "Exact and approximate maximum likelihood localization algorithms". In: *IEEE Transactions on Vehicular Technology* 55.1 (2006), pp. 10–16.

[22] Pi-Chun Chen. "A non-line-of-sight error mitigation algorithm in location estimation". In: *WCNC. 1999 IEEE Wireless Communications and Networking Conference (Cat. No.99TH8466)*. Vol. 1. 1999, 316–320 vol.1.

[23] Y. T. Chan and K. C. Ho. "A simple and efficient estimator for hyperbolic location". In: *IEEE Transactions on Signal Processing* 42.8 (1994), pp. 1905–1915.

[24] Li Cong and Weihua Zhuang. "Hybrid TDOA/AOA mobile user location for wideband CDMA cellular systems". In: *IEEE Transactions on Wireless Communications* 1.3 (2002), pp. 439–447.

[25] J. J. Caffery and G. L. Stuber. "Overview of radiolocation in CDMA cellular systems". In: *IEEE Communications Magazine* 36.4 (1998), pp. 38–45.

[26] Yiu-Tong Chan, Wing-Yue Tsui, Hing-Cheung So and Pak-chung Ching. "Time-of-arrival based localization under NLOS conditions". In: *IEEE Transactions on Vehicular Technology* 55.1 (2006), pp. 17–24.

AppendixA

CDL Channel Model

According to [10], parameters of different CDL models are listed as below.

Cluster #	Normalized delay	Power in [dB]	AOD in [°]	AOA in [°]	ZOD in [°]	ZOA in [°]
1	0.0000	-13.4	-178.1	51.3	50.2	125.4
2	0.3819	0	-4.2	-152.7	93.2	91.3
3	0.4025	-2.2	-4.2	-152.7	93.2	91.3
4	0.5868	-4	-4.2	-152.7	93.2	91.3
5	0.4610	-6	90.2	76.6	122	94
6	0.5375	-8.2	90.2	76.6	122	94
7	0.6708	-9.9	90.2	76.6	122	94
8	0.5750	-10.5	121.5	-1.8	150.2	47.1
9	0.7618	-7.5	-81.7	-41.9	55.2	56
10	1.5375	-15.9	158.4	94.2	26.4	30.1
11	1.8978	-6.6	-83	51.9	126.4	58.8
12	2.2242	-16.7	134.8	-115.9	171.6	26
13	2.1718	-12.4	-153	26.6	151.4	49.2
14	2.4942	-15.2	-172	76.6	157.2	143.1
15	2.5119	-10.8	-129.9	-7	47.2	117.4
16	3.0582	-11.3	-136	-23	40.4	122.7
17	4.0810	-12.7	165.4	-47.2	43.3	123.2
18	4.4579	-16.2	148.4	110.4	161.8	32.6
19	4.5695	-18.3	132.7	144.5	10.8	27.2
20	4.7966	-18.9	-118.6	155.3	16.7	15.2
21	5.0066	-16.6	-154.1	102	171.7	146
22	5.3043	-19.9	126.5	-151.8	22.7	150.7
23	9.6586	-29.7	-56.2	55.2	144.9	156.1
Per-Cluster Parameters						
Parameter	c_{ASD} in [°]		c_{ASA} in [°]	c_{ZSD} in [°]	c_{ZSA} in [°]	XPR in [dB]
Value	5		11	3	3	10

Figure A.1: CDL-A [10].

Cluster #	Normalized delay	Power in [dB]	AOD in [°]	AOA in [°]	ZOD in [°]	ZOA in [°]
1	0.0000	0	9.3	-173.3	105.8	78.9
2	0.1072	-2.2	9.3	-173.3	105.8	78.9
3	0.2155	-4	9.3	-173.3	105.8	78.9
4	0.2095	-3.2	-34.1	125.5	115.3	63.3
5	0.2870	-9.8	-65.4	-88.0	119.3	59.9
6	0.2986	-1.2	-11.4	155.1	103.2	67.5
7	0.3752	-3.4	-11.4	155.1	103.2	67.5
8	0.5055	-5.2	-11.4	155.1	103.2	67.5
9	0.3681	-7.6	-67.2	-89.8	118.2	82.6
10	0.3697	-3	52.5	132.1	102.0	66.3
11	0.5700	-8.9	-72	-83.6	100.4	61.6
12	0.5283	-9	74.3	95.3	98.3	58.0
13	1.1021	-4.8	-52.2	103.7	103.4	78.2
14	1.2756	-5.7	-50.5	-87.8	102.5	82.0
15	1.5474	-7.5	61.4	-92.5	101.4	62.4
16	1.7842	-1.9	30.6	-139.1	103.0	78.0
17	2.0169	-7.6	-72.5	-90.6	100.0	60.9
18	2.8294	-12.2	-90.6	58.6	115.2	82.9
19	3.0219	-9.8	-77.6	-79.0	100.5	60.8
20	3.6187	-11.4	-82.6	65.8	119.6	57.3
21	4.1067	-14.9	-103.6	52.7	118.7	59.9
22	4.2790	-9.2	75.6	88.7	117.8	60.1
23	4.7834	-11.3	-77.6	-60.4	115.7	62.3
Per-Cluster Parameters						
Parameter	c_{ASD} in [°]		c_{ASA} in [°]	c_{ZSD} in [°]	c_{ZSA} in [°]	XPR in [dB]
Value	10		22	3	7	8

Figure A.2: CDL-B [10].

Cluster #	Normalized delay	Power in [dB]	AOD in [°]	AOA in [°]	ZOD in [°]	ZOA in [°]
1	0	-4.4	-46.6	-101	97.2	87.6
2	0.2099	-1.2	-22.8	120	98.6	72.1
3	0.2219	-3.5	-22.8	120	98.6	72.1
4	0.2329	-5.2	-22.8	120	98.6	72.1
5	0.2176	-2.5	-40.7	-127.5	100.6	70.1
6	0.6366	0	0.3	170.4	99.2	75.3
7	0.6448	-2.2	0.3	170.4	99.2	75.3
8	0.6560	-3.9	0.3	170.4	99.2	75.3
9	0.6584	-7.4	73.1	55.4	105.2	67.4
10	0.7935	-7.1	-64.5	66.5	95.3	63.8
11	0.8213	-10.7	80.2	-48.1	106.1	71.4
12	0.9336	-11.1	-97.1	46.9	93.5	60.5
13	1.2285	-5.1	-55.3	68.1	103.7	90.6
14	1.3083	-6.8	-64.3	-68.7	104.2	60.1
15	2.1704	-8.7	-78.5	81.5	93.0	61.0
16	2.7105	-13.2	102.7	30.7	104.2	100.7
17	4.2589	-13.9	99.2	-16.4	94.9	62.3
18	4.6003	-13.9	88.8	3.8	93.1	66.7
19	5.4902	-15.8	-101.9	-13.7	92.2	52.9
20	5.6077	-17.1	92.2	9.7	106.7	61.8
21	6.3065	-16	93.3	5.6	93.0	51.9
22	6.6374	-15.7	106.6	0.7	92.9	61.7
23	7.0427	-21.6	119.5	-21.9	105.2	58
24	8.6523	-22.8	-123.8	33.6	107.8	57
Per-Cluster Parameters						
Parameter	c_{ASD} in [°]		c_{ASA} in [°]	c_{ZSD} in [°]	c_{ZSA} in [°]	XPR in [dB]
Value	2		15	3	7	7

Figure A.3: CDL-C [10].

Cluster #	Cluster PAS	Normalized Delay	Power in [dB]	AOD in [°]	AOA in [°]	ZOD in [°]	ZOA in [°]
1	Specular(LOS path)	0	-0.2	0	-180	98.5	81.5
	Laplacian	0	-13.5	0	-180	98.5	81.5
2	Laplacian	0.035	-18.8	89.2	89.2	85.5	86.9
3	Laplacian	0.612	-21	89.2	89.2	85.5	86.9
4	Laplacian	1.363	-22.8	89.2	89.2	85.5	86.9
5	Laplacian	1.405	-17.9	13	163	97.5	79.4
6	Laplacian	1.804	-20.1	13	163	97.5	79.4
7	Laplacian	2.596	-21.9	13	163	97.5	79.4
8	Laplacian	1.775	-22.9	34.6	-137	98.5	78.2
9	Laplacian	4.042	-27.8	-64.5	74.5	88.4	73.6
10	Laplacian	7.937	-23.6	-32.9	127.7	91.3	78.3
11	Laplacian	9.424	-24.8	52.6	-119.6	103.8	87
12	Laplacian	9.708	-30.0	-132.1	-9.1	80.3	70.6
13	Laplacian	12.525	-27.7	77.2	-83.8	86.5	72.9
Per-Cluster Parameters							
Parameter		c_{ASD} in [°]	c_{ASA} in [°]	c_{ZSD} in [°]	c_{ZSA} in [°]	XPR in [dB]	
Value		5	8	3	3	11	

Figure A.4: CDL-D [10].

Cluster #	Cluster PAS	Normalized Delay	Power in [dB]	AOD in [°]	AOA in [°]	ZOD in [°]	ZOA in [°]
1	Specular (LOS path)	0.000	-0.03	0	-180	99.6	80.4
	Laplacian	0.000	-22.03	0	-180	99.6	80.4
2	Laplacian	0.5133	-15.8	57.5	18.2	104.2	80.4
3	Laplacian	0.5440	-18.1	57.5	18.2	104.2	80.4
4	Laplacian	0.5630	-19.8	57.5	18.2	104.2	80.4
5	Laplacian	0.5440	-22.9	-20.1	101.8	99.4	80.8
6	Laplacian	0.7112	-22.4	16.2	112.9	100.8	86.3
7	Laplacian	1.9092	-18.6	9.3	-155.5	98.8	82.7
8	Laplacian	1.9293	-20.8	9.3	-155.5	98.8	82.7
9	Laplacian	1.9589	-22.6	9.3	-155.5	98.8	82.7
10	Laplacian	2.6426	-22.3	19	-143.3	100.8	82.9
11	Laplacian	3.7136	-25.6	32.7	-94.7	96.4	88
12	Laplacian	5.4524	-20.2	0.5	147	98.9	81
13	Laplacian	12.0034	-29.8	55.9	-36.2	95.6	88.6
14	Laplacian	20.6419	-29.2	57.6	-26	104.6	78.3
Per-Cluster Parameters							
Parameter		c_{ASD} in [°]	c_{ASA} in [°]	c_{ZSD} in [°]	c_{ZSA} in [°]	XPR in [dB]	
Value		5	11	3	7	8	

Figure A.5: CDL-E [10].

LUND
UNIVERSITY